Single Molecule Fluorescence Spectroscopy at Ambient Temperature

W. Patrick Ambrose,[†] Peter M. Goodwin,[†] James H. Jett,[‡] Alan Van Orden,[†,§] James H. Werner,[†] and Richard A. Keller*[,†]

Chemical Science and Technology Division and Life Sciences Division, MS M888, Los Alamos National Laboratory, Los Alamos, New Mexico 87545

Received February 18, 1999 (Revised Manuscript Received July 16, 1999)

Contents

I. Introduction 2929
II. Single Molecule Spectroscopy in Flowing Solutions 2931
  A. Hydrodynamic Focusing 2931
  B. Pulsed Excitation and Time-Correlated Detection 2931
  C. Photobleaching To Reduce Background from Fluorescent Impurities 2931
  D. Apparatus 2932
  E. Data Analysis 2933
  F. Data Simulations 2934
  G. Results 2934
    1. Single Molecule Detection 2934
    2. Identification at the Single Molecule Level 2936
  H. Applications 2938
    1. DNA Sequencing 2938
    2. DNA Fragment Sizing 2939
    3. Two Color Homogeneous Assay for Probe/Target Binding 2941
    4. Single Molecule Electrophoresis 2942
III. Single Molecule Spectroscopy on Levitated Microdroplets 2943
IV. Confocal Excitation and Detection for Single Molecule Spectroscopy 2944
  A. Single Molecule Detection 2944
  B. Fluorescence Correlation Spectroscopy in Liquids 2945
V. Single Molecule Spectroscopy in Microcapillaries and Microstructures 2947
VI. Single Molecule Spectroscopy by Two-Photon Excitation 2948
VII. Single Molecule Imaging under Ambient Conditions with Cameras 2950
  A. Overview 2950
  B. Technical Challenges and Solutions 2950
  C. Sensitive Cameras 2951
  D. Translational Motion 2952
  E. Reorientational Motion 2952
  F. Intensity Fluctuations and Chemical Kinetics 2953
VIII. References 2953

I. Introduction

Analytical chemistry has entered a new era. Individual molecules can be detected, identified, counted, and, in some cases, their physical and chemical properties measured. Big advances have been made in the detection of single fluorescent molecules in liquids at room temperature since the first successful detection of a molecule labeled with 80−100 fluorescein fluorophores in 1976.[1] Our quest for the detection of single fluorophore molecules began with the work of Dovichi in 1983[2,3] and progressed until we demonstrated the detection of single molecules in 1990.[4] The first single molecule detected and the most heavily studied is Rhodamine 6G (R6G). A common derivative, suitable for labeling, is tetramethylrhodamine isothiocyanate (TRITC). The structures of both molecules are shown in Figure 1. This review focuses primarily on the spectroscopy of single molecules containing a single fluorophore. A number of groups have demonstrated the ability to detect and identify single fluorophore molecules under ambient conditions by laser-induced fluorescence.[4−30] Progress in single molecule detection is summarized in several review articles.[31−42] Single molecule measurements are a significant advancement in detection technology. Measurement capability is at the core of all physical investigations. Increased measurement capabilities have led to the discovery and understanding of many new physical phenomena. A trend in modern analytical and material sciences is to make devices smaller and faster with the ultimate goal of devices at the molecular level. At this level, sensitive detection is a major issue.

The ability to make measurements at the single molecule level leads to a detailed understanding of systems that would be difficult or impossible with bulk measurements where the properties of individual molecules are hidden in ensemble averages. At the single molecule level heterogeneities, properties of trace constituents (including rare conformations), and differences in reaction pathways may become visible. Often trace constituents or minor reaction pathways are the most important in determining the properties of a system.

As a highly fluorescent molecule transits a laser beam tuned to an optical transition of the molecule, it is continuously cycled between the ground and an excited electronic state emitting a photon on most cycles. For fluorescence, the maximum number of

* To whom correspondence should be addressed.
[†] Chemical Science and Technology Division.
[‡] Life Sciences Division.
[§] Present address: Department of Chemistry, Colorado State University, Fort Collins, CO 80523.

10.1021/cr980132z CCC: $35.00
Published on Web 09/23/1999

William Patrick Ambrose (3rd from right) is interested in challenging research in ultrasensitive optical detection, including single molecule detection in solids, in liquids, and at interfaces. He obtained his Ph.D. in condensed matter physics from Cornell in 1989 with Prof. A. J. Sievers (combined IR and far-IR laser spectroscopy and high-resolution FTIR of internal and external vibrational modes of small molecules in solids at liquid helium temperatures). Since then, Pat has been a Visiting Scientist at IBM's Almaden Research Center working with W. E. Moerner (1989–1991; including single molecule spectroscopy at low temperatures) and a Director's Funded Postdoctoral Fellow at Los Alamos National Laboratory with R. A. Keller (LANL 1991–1993; including single molecule detection in liquids and on surfaces). Since 1993, Pat has been a staff member at LANL investigating various forms of sensitive fluorescence imaging in single molecule studies. His accomplishments are recognized in a LANL Individual Distinguished Performance Award (1994) and a LANL Team Distinguished Performance Award (1995). He is also a co-investigator on a R&D 100 Award for "Rapid Size Analysis of Individual DNA Fragments", June 1997.

Peter M. Goodwin (2nd from left) received his B.S. degree in physics from the California Institute of Technology in 1980 and a Ph.D. in applied and engineering physics from Cornell University in 1989. He held postdoctoral positions at the IBM Technology Laboratory, Endicott, NY, and at Los Alamos National Laboratory, Los Alamos, NM. He is currently a staff member in the Chemical Science and Technology Division at Los Alamos. His research interests are in the areas of laser spectroscopy and ultrasensitive detection.

James Jett (left), a Laboratory Fellow, received a B.S. in mathematics (with honors) and a M.S. in physics in 1961 from the University of New Mexico and a Ph.D. in experimental nuclear physics in 1969 from the University of Colorado. During a break in his education, he spent three years in the Navy as an officer at the Bureau of Ships. In 1969 he came to Los Alamos as a Postdoctoral fellow in the low energy nuclear physics group. After a short appointment in a nuclear safeguards group, he transferred to what is now the Life Sciences Division at Los Alamos. In the Life Sciences Division he has been involved in a number of research areas ranging from quantification of prophage induction to the development of new measurement techniques in flow cytometry. Jett is the Principal Investigator of the National Flow Cytometry Resource, a NIH funded resource that develops new techniques in flow cytometry as well as serves the user community. Technical interests include data acquisition system development, ultrasensitive measurement techniques based on flow cytometry, and application of the techniques in cell biology and the Human Genome project. He has published more than 20 papers in nuclear physics and 70 papers in biophysics/flow cytometry.

Alan Van Orden (3rd from left) was born in Champaign, IL, in 1966 and was raised in Pocatello, ID. He earned a B.S. degree in Chemistry from Brigham Young University (Provo, UT) in 1990 and a Ph.D. in physical chemistry from the University of California—Berkeley in 1996, under the supervision of Professor Richard J. Saykally. From 1996 to 1999, he was a postdoctoral research associate at the Los Alamos National Laboratory, where he worked with Richard A. Keller and co-workers on the development of new techniques for the detection and identification of single molecules in solution. At present, he is Assistant Professor of Chemistry at Colorado State University (Fort Collins). His research and teaching interests are directed toward the study of single molecules, biological systems, and nanostructured materials using ultrasensitive laser-based spectroscopy and microscopy techniques.

James Werner (right) received his B.S. degree in applied physics from the California Institute of Technology in 1992. He earned a Ph.D. degree in applied and engineering physics from Cornell University in 1998 and since that time has been a postdoctoral research associate with Los Alamos National Laboratory. His current research involves biological applications of single molecule fluorescence detection.

Richard A. Keller (2nd from right) received his B.S. degree from Allegheny College in 1956 and his Ph.D. from the University of California, Berkeley, in 1961. Keller was on the faculty at the University of Oregon from 1960 to 1963 and at the National Bureau of Standards, Washington, DC, from 1963 to 1976. Keller joined Los Alamos National Laboratory in 1976. He is currently a Laboratory Fellow in the Chemical Science and Technology Division at Los Alamos. Keller is the recipient of the 1993 ACS Division of Analytical Chemistry Award for Spectrochemical Analysis and the 1996 Lester W. Strock Award from the Society for Applied Spectroscopy. He was elected to the Society of Fluorescence in October 1997. Keller's research interests are in the development and characterization of new ultrasensitive analytical techniques. In particular, he is interested in the application of single molecule detection to analytical measurements.

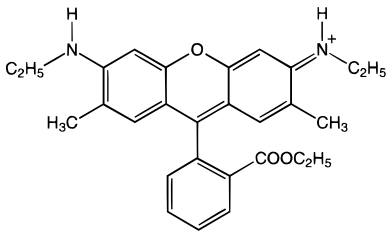

Rhodamine 6G

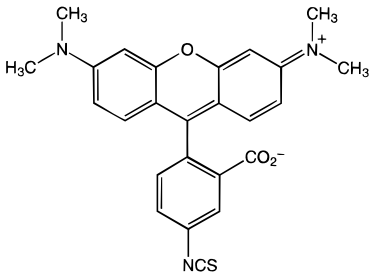

5-TRITC

Figure 1. Structures of the fluorescent dye molecules Rhodamine 6G (R6G) and tetramethyrhodamine isothiocyanate (TRITC).

photons that can be emitted is given by

$$N_{max} = \tau_t/\tau_f \quad (1)$$

Here, τ_t is the transit time across the laser beam and τ_f is the fluorescence lifetime. The fluorescence lifetime enters because the molecule must relax before it can be re-excited. For typical values of τ_t = 1 ms and τ_f = 1 ns, $N_{max} = 10^6$. Unfortunately, even very stable molecules photodecompose before absorbing $\sim 10^5$ photons.[43–47] Sensitive optical systems used in single molecule studies have a fluorescence photon detection efficiency of $\sim$1%.[48] The result is that the signature of a single molecule crossing the laser beam is a burst of 10−1000 detected photons or photoelectrons (burst size). The fact that the signal comes in bursts, rather than randomly distributed in time, is used to distinguish the signal from background.

Single molecule detection is not as much a sensitivity issue as it is a background issue. A fluorescence burst characteristic of a single molecule must be detected on top of the background associated with the

solvent. The background is minimized by using small probe volumes because the signal from a single molecule is independent of the probe volume while the background is proportional to the probe volume. Essentially, all demonstrations of single molecule detection are based upon the use of probe volumes of 10 pL or less. Five approaches to obtaining small probe volumes are described below: (1) hydrodynamically focused sample streams crossed with a tightly focused excitation laser beam and imaging detection optics to attain probe volumes of ~1 pL (10 μm × 10 μm × 10 μm) (section II); (2) levitated microdroplets of volume 1 fL−1 pL (1−10 μm diameter) (section III); (3) confocal excitation and detection with one- and two-photon excitation to attain probe volumes of ~1 fL (1 μm × 1 μm × 1 μm) (sections IV and VI); (4) microbore capillaries and microchannels to attain probe volumes 1 fL−1 pL (section V); (5) wide field illumination of molecules on surfaces or in thin films with high-resolution microscope imaging to attain detection areas of ~0.1 μm^2 (section VII).

In this article we describe these approaches to single fluorescent molecule detection and applications in analytical and physical chemistry. The use of near-field excitation to attain attoliter probe volumes (NSOM) and single molecule spectroscopy by surface enhanced Raman scattering (SERS) are subjects of other reviews in this issue and will not be discussed here.

II. Single Molecule Spectroscopy in Flowing Solutions

II.A. Hydrodynamic Focusing

The importance of using small probe volumes to distinguish fluorescence from a single molecule from background emission from the solvent was discussed in the Introduction. Hydrodynamic focusing provides a means of introducing sample into small probe volumes and plays a major role in single molecule detection.[17,49] A diagram of an apparatus using hydrodynamic focusing for single molecule detection is shown in Figure 2. Hydrodynamic focusing occurs

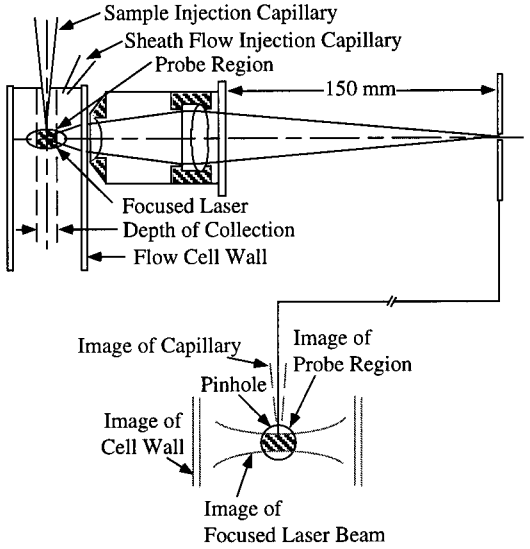

Figure 2. Apparatus for single molecule detection in hydrodynamically focused sample streams. Reprinted with permission from: Li, L.-Q.; Davis, L. M. *Appl. Opt.* **1995**, *34*, 3208−3217. Copyright 1995 Optical Society of America.

when a sample stream is introduced into a rapidly flowing sheath stream from a small orifice.[50] During focusing, the sample steam accelerates to catch up with the sheath stream keeping the volume flow rate of the sample constant. Conservation of mass requires the diameter of the sample stream to decrease. Hydrodynamic focusing results in sample stream diameters ranging from 1 to 20 μm, determined by radial diffusion of the analyte molecules into the sheath stream.[51] The focused sample stream is typically in the center of the flow cell where the Poiseville flow profile is relatively constant. An additional advantage of focused flow is that the sample stream is far from the cell walls minimizing problems associated with scattered light, adsorption of analyte to the cell walls, and desorption of impurity molecules into the detection volume.

The excitation laser is focused to a diameter of ~10 μm. The emitted light is collected by a high numerical aperture microscope objective, passed through a slit (spatial filter), and imaged onto a sensitive detector. The probe volume can be approximated as a cylinder with a diameter of the focused laser beam and length equal to the slit width divided by the magnification of the microscope objective. Typical probe volumes used with hydrodynamic focusing are 1−10 pL.

II.B. Pulsed Excitation and Time-Correlated Detection

If required, additional suppression of background associated with Raman and Rayleigh scattering of the laser excitation light can be attained by time-correlated, single photon counting (TCSPC).[52] Mode-locked lasers (Ar^+, dye, Nd:YAG, diode) are used to generate subnanosecond excitation pulses. Fluorescence decay times of highly fluorescent molecules typically range from 2 to 5 ns. A time-gate on a time-to-amplitude converter (TAC) and single channel analyzer (SCA) is set to process only photons arriving with a delay >1 ns after the excitation pulse. This results in a reduction of the detected Raman and Rayleigh scattered light of more than 2 orders of magnitude.[4] The effect of time-gating on single molecule detection is shown in Figure 3. The use of pulsed excitation and time-correlated analysis results in the detection of photon bursts associated with the passage of single molecules through pL probe volumes with excellent signal-to-background.[4,8,10] An additional benefit of TCSPC is the ability to measure the fluorescence decay time for single molecules as they flow through the detection volume (see section II.G.2.b).

II.C. Photobleaching To Reduce Background from Fluorescent Impurities

Even with small probe volumes and TCSPC detection, there is often significant background emission associated with fluorescent impurities in the solvent. This is especially true for buffer solutions when extreme measures are not used to remove fluorescent impurities. In practice, background due to fluorescent impurities often sets detection limits. This background can be reduced 1 order of magnitude or more

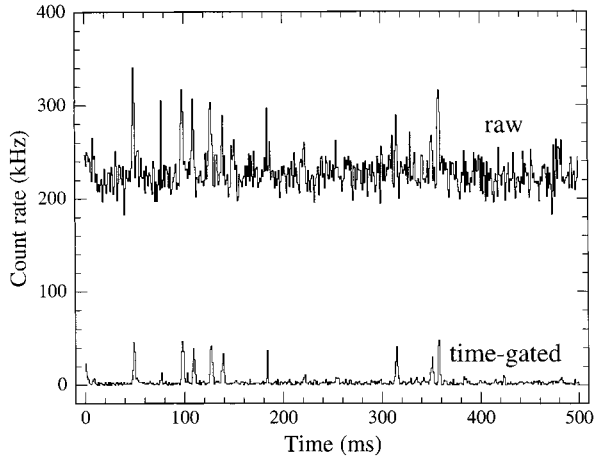

Figure 3. Detection of single R6G molecules using pulsed excitation and time-correlated single photon counting (TCSPC) to discriminate against water Raman scattering background. R6G molecules dissolved in water flowed through a 16 μm e^{-2} diameter 514.5 nm mode-locked Ar^+ excitation laser beam (~200 ps pulse width, 82 MHz repetition rate, 30 mW average power). Fluorescence emission was detected through a 550 ± 30 nm band-pass filter using a single photon counting avalanche photodiode. Top curve (raw) is 500 ms of raw TCSPC data binned into 1 ms intervals. Bottom curve (time-gated) is the same TCSPC data processed to remove photons detected within ~1 ns of the excitation laser pulse (primarily due to Raman scattered excitation laser light). Fluorescence photon bursts from single R6G molecules (~40 kHz peaks) are clearly evident in the time-gated TCSPC data.

by photobleaching the sheath fluid before introducing the analyte.[53] The sheath fluid is flowed through a 1 m long, 0.5 mm i.d. capillary (photolysis cell) on the way to the flow cuvette. A fraction of the excitation laser light is split off and passed collinearly through the capillary. Interfering fluorescent impurity molecules absorb laser light and are photobleached as they pass through the photolysis cell. The effect of photobleaching on the detection of tetramethylrhodamine isothiocyanate (TRITC) single molecules dissolved in buffer is shown in Figure 4. Without photobleaching most of the bursts observed are from fluorescent impurities in the sheath buffer.

II.D. Apparatus

Apparatus for single molecule detection in hydrodynamically focused streams are described in detail by Goodwin[49] and Li.[17] A typical apparatus is shown in Figure 2. Briefly, samples are introduced into the center of a 250 μm × 250 μm, square bore sheath flow cell from a small bore capillary (i.d. 1−10 μm; o.d. ~100 μm) inserted into the flow cell. One wall of the flow cell is fabricated with a microscope coverslip thickness (~170 μm) to match the working distance of the fluorescence collection objective. Output from a mode-locked laser is focused to a beam waist of ~10 μm and passed through the flow cell ~50 μm downstream from the capillary orifice. Light is collected by a high numerical aperture (NA) microscope objective (40×, NA 0.85), placed at 90° to the excitation and sample flow axes, and imaged onto a 600 μm slit that acts as a spatial filter to limit the probe volume to ~1 pL. An optical collection efficiency of ~10% was measured for this combination of flow cell and

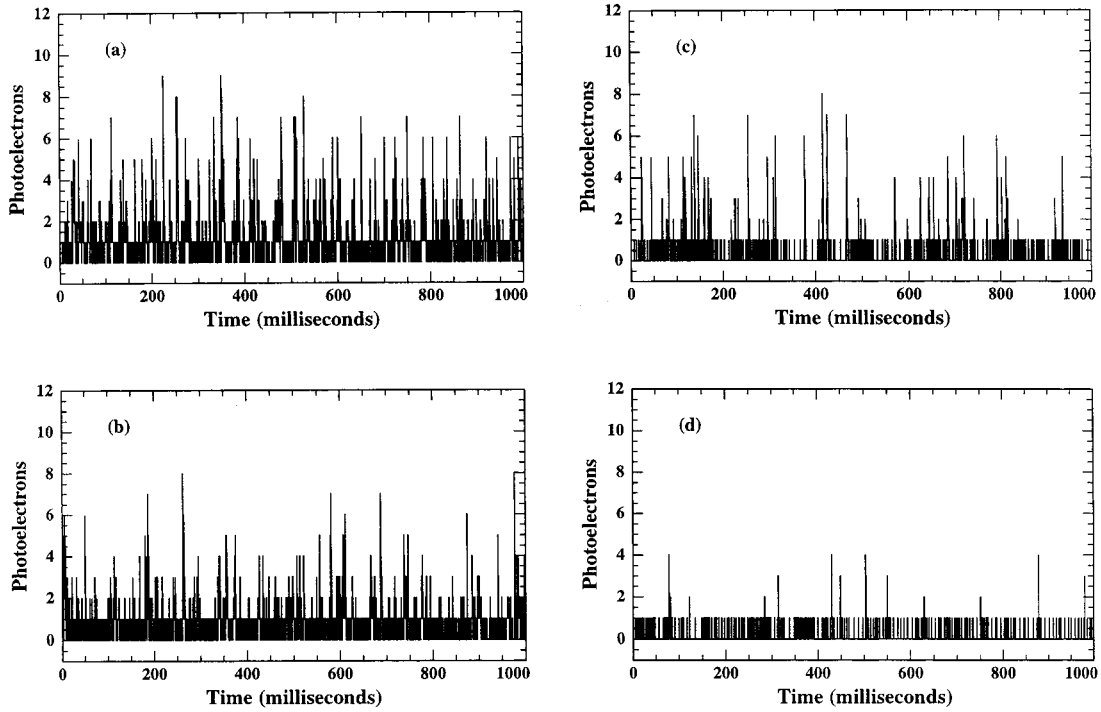

Figure 4. Laser photolysis of sheath buffer to remove fluorescent impurities. Time sequences of detected fluorescence photons (photoelectrons) from TRITC electrokinetically introduced into a sheath flow are shown. Sheath buffer was delivered through a laser photolysis chamber (~180 μL volume) at 10 μL/min. TRITC was delivered into the sheath flow downstream of the photolysis chamber from a capillary located ~50 μm upstream of the detection volume. Key: (a) sample stream on with no photolysis; (b) sample stream off with no photolysis; (c) sample stream on with photolysis; (d) sample stream off with photolysis. The photolysis source was a mode-locked dye laser operating at 554 nm with an average power of 220 mW. Reprinted from: Affleck, R. L.; Ambrose, W. P.; Demas, J. N.; Goodwin, P. M.; Schecker, J. A.; Wu, M.; Keller, R. A. *Anal. Chem.* **1996**, *68*, 2270−2276. Copyright 1996 American Chemical Society.

microscope objective.[48] Light transmitted by the slit is passed through appropriate optical filters to reduce Raman and Rayleigh scattered light and focused onto the active area of a high sensitivity photomultiplier tube (PMT) or a single photon-counting avalanche photodiode (SAPD). Photon counting SAPDs are a new class of photon detectors that have better than 40% efficiency in the mid-visible spectral range. Use of SAPDs for single molecule detection is described in detail by Li and Davis.[8] The overall light detection efficiency (photons detected/photons emitted) is ~1%.[49] The detected photons are processed using TCSPC to reject photoelectron pulses from Raman and Rayleigh scatter.[4,8,10,54]

II.E. Data Analysis

Analysis methods have evolved along with experimental techniques and the quality of single molecule fluorescence data have improved. Autocorrelation of the time history of the count rate is an extremely sensitive method for detecting the presence of photon bursts associated with the passage of single fluorescent molecules through the detection volume.[55] The burst data are processed to give the autocorrelation function, $G(\tau)$:

$$G(\tau) = \sum_{t=0}^{N-1} g(t)g(t+\tau) \qquad (2)$$

N is the total number of time intervals in the data, $g(t)$ is the number of photoelectrons detected during the time interval, $[t, t + \Delta t]$, and $g(t + \tau)$ is the number of photoelectrons detected in Δt at a later time, $t + \tau$. A finite width peak in the autocorrelation centered at zero delay indicates the detection of photon bursts from single molecules. A typical autocorrelation function is shown in Figure 5. The width

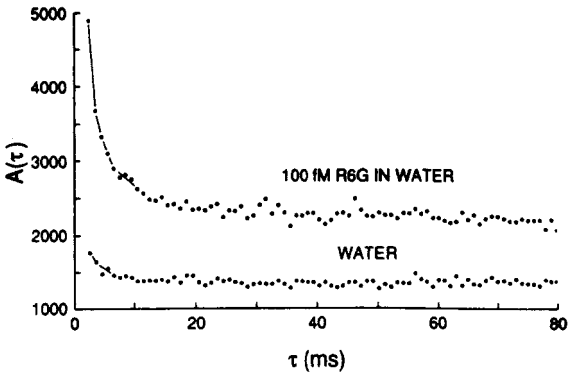

Figure 5. Autocorrelation functions for water and a 100 fM solution of R6G. The autocorrelation was computed over 132 s of data. The $A(0)$ points are off scale. The presence of single molecules of R6G is evidenced by the nonrandom correlation at small values of τ. Reprinted with permission from: Shera, E. B.; Seitzinger, N. K.; Davis, L. M.; Keller, R. A.; Soper, S. A. *Chem. Phys. Lett.* **1990**, *174*, 553−557. Copyright 1990 Elsevier Science.

of the autocorrelation peak is a measure of the average temporal coherence length of the fluorescence bursts. For analyte molecules that do not photobleach significantly, this is a measure of the molecules' transit time across the detection volume. Photobleaching and diffusion reduce the average residence time of the fluorescent molecules in the excitation laser beam and are reflected in the width and shape of the autocorrelation peak.

While autocorrelation analysis is useful for detecting the presence of and analyzing the average properties of single molecule fluorescence bursts in a data steam, it is not well suited for detecting and analyzing individual fluorescence bursts, one at a time. The first demonstration of fluorescence detection of single fluorophore molecules (R6G) in solution used a weighted-quadratic-sum filter, $S(t)$, to find individual, single molecule fluorescence bursts in the data stream:[4]

$$S(t) = \sum_{\tau=0}^{k-1} \omega(\tau)\, g(t+\tau)^2 \qquad (3)$$

Here, $\omega(\tau)$ is a weighting function chosen to discriminate between a single molecule fluorescence burst and random fluctuations in the background. An asymmetric triangular ramp $\omega(\tau) = (\tau + 1)/k$ for $\tau = 0$ to $k - 1$ and $\omega(\tau) = 0$ otherwise was used to mimic the shape of the fluorescence burst from a molecule whose fluorescence emission rate increases as it approaches the more intense center of the excitation beam but abruptly photobleaches before reaching the center. This was appropriate for the relatively intense excitation and long transit times used in this work.[4] k was chosen so that $k\Delta t$ was approximately the transit time of molecules through the detection volume. The passage of a single fluorescent molecule through the detection volume is recorded as a spike rising above a preset discrimination threshold in the filtered data, $S(t)$ (see section II.G.2.a).

Another approach[54,56−59] to data collection and analysis that has proven useful, especially, when single molecule fluorescence decay lifetimes are to be measured, is described here. For each event (i.e., a photon detected within a time-window suitably delayed with respect to the excitation laser pulse), three pieces of information are recorded: (1) the event number; (2) the "microscopic" time elapsed between the excitation laser pulse and the detection of the photon; (3) the "macroscopic" time between the current and the previous event. Figure 6 shows a segment of raw data (filled circles) recorded during the detection of fluorescence bursts from single Rhodamine-110 molecules dissolved in water. The horizontal axis denotes the event number and the vertical axis the macroscopic time (number of 100 kHz clock ticks) between successive events. For the data shown in Figure 6, a fluorescence burst is evidenced by a series of successive events recorded at a high rate (2−20 kHz) compared to the background detection rate (0.3−0.4 kHz). A procedure to search the data for fluorescence bursts starts by smoothing the raw data as shown in the figure by the solid curve. A threshold level is chosen (50 clock ticks or 0.5 ms for the data shown), and the smoothed data are searched for runs of successive points less than or equal to this level. A series of five or more smoothed data points at or below the threshold was taken to be a fluorescence burst. The search algo-

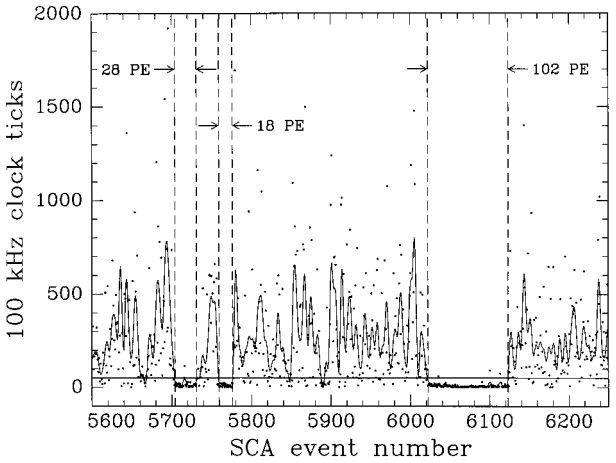

Figure 6. Segment of fluorescence burst data collected from an ultradilute solution of Rh-110 in water. Experimental conditions: excitation source, mode-locked Ar^+ laser (10 mW average power at 496 nm, 82 MHz pulse repetition rate, 200 ps pulse width, 13 μm e^{-2} beam diameter); sample, 3×10^{-14} M Rh-110 dissolved in ultrapure water. The horizontal axis denotes the event number assigned to the photon detected within a time window defined by a single channel analyzer (SCA) equipped time-to-amplitude converter. The vertical axis denotes the time between successive events in units of 100 kHz clock ticks. Raw fluorescence data are shown as filled circles. The solid curve is the result of a fast Fourier transform based five point smoothing of the raw data. A threshold of 50 clock ticks (0.5 ms) is indicated by the horizontal line. Three fluorescence bursts ≥5 photoelectrons in size found by the search algorithm are delineated with vertical dashed lines. Reprinted with permission from: Goodwin, P. M.; Wilkerson, C. W., Jr.; Ambrose, W. P.; Keller, R. A. *Proc. SPIE* **1993**, *1895*, 79−89. Copyright 1993 International Society for Optical Engineering.

rithm found three bursts ≥5 photoelectrons in the data shown in the figure. The microscopic arrival times (with respect to the laser pulse) of photons detected within the fluorescence burst can be used for single molecule fluorescence lifetime analysis (see section II.G.2.b).

To reduce contributions from background bursts and accidental coincidences (two or more analyte molecules in the detection volume at the same time) the bursts are time filtered and bursts with significantly longer or shorter durations than the mean transit time across the detection volume are rejected.[60]

11.F. Data Simulations

Modeling calculations to simulate a data stream are very informative.[5,17,49,54,59,61−63] Input parameters include the following: sample introduction rate; sheath flow velocity; analyte absorption cross section; fluorescence quantum yield; photobleaching quantum yield; optical saturation intensity; analyte diffusion constant; excitation irradiance; spatial dependence of excitation and collection efficiency; transmission of collection optics and optical filters; quantum efficiency and the dead time of the photon detector. A molecule's transit through the detection region is divided into a series of small steps. At each step a Monte Carlo approach[5,54,61] is used to determine if the molecule absorbs a photon, the molecule emits a photon, the emitted photon is detected, and photobleaching occurs. Axial and radial diffusion are calculated at each step to give the molecule's coordinates for the next simulation step. The simulation yields the detection efficiency (molecules detected/molecules introduced) and the burst size distribution for the sample. Figure 7 demonstrates that the

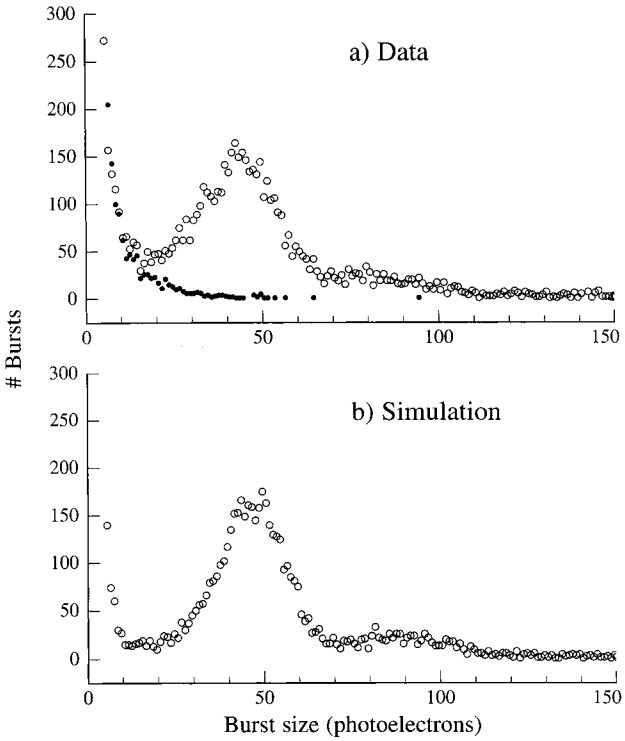

Figure 7. Experimental and simulated photon burst size distributions (BSDs). Panel a: open circles, measured BSD for single TRITC molecules delivered electrokinetically from a drawn capillary into a sheath flow through a ~3 pL detection volume; filled circles, background BSD measured with the sample stream misaligned with respect to the detection volume. Panel b: BSD compiled from synthetic data generated by a Monte Carlo simulation of the experiment. Each BSD was compiled from 64 s of data. Reprinted with permission from: Goodwin, P. M.; Affleck, R. L.; Ambrose, W. P.; Demas, J. N.; Jett, J. H.; Martin, J. C.; Reha-Krantz, L. J.; Semin, D. J.; Schecker, J. A.; Wu, M.; Keller, R. A. *Exp. Tech. Phys.* **1995**, *41*, 279−294. Copyright 1995 Huethig.

calculated burst size distribution is in excellent agreement with the measured burst size distribution.[49] The parameters used for the simulation calculation shown in Figure 7 are given in Table 1. The simulation calculations provide physical insight to the experimental detection process and predict the effect of changes in the basic photophysical and experimental parameters. More formal approaches to data simulation yield similar results.[59,62,63]

II.G. Results

II.G.1. Single Molecule Detection

One second of data showing photon bursts from R6G molecules desorbing from an optically trapped microsphere is displayed in Figure 8a.[60] Each peak represents the passage of a single R6G molecule through the detection volume. For comparison, data

Table 1. Parameters Used for the Data Simulation Calculations

TRITC absorption cross section at 554 nm[a]	3.1×10^{-16} cm^2
TRITC fluorescence quantum yield[233]	0.28
TRITC photodestruction quantum yield[43]	6×10^{-6}
TRITC diffusion coefficient[b]	3.3×10^{-6} cm^2 s^{-1}
TRITC saturation intensity[c]	4×10^4 W cm^{-2}
average excitation laser power	20×10^{-3} W
excitation laser beam e^{-2} diameter	14 μm
sample flow velocity[d]	0.79 cm s^{-1}
absolute fluorescence photon detection efficiency	1×10^{-2}
background count rate/W excitation power	1.4×10^5 s^{-1} W^{-1}

[a] Estimated from the TRITC absorption spectrum and the reported[43] absorption cross section at 515 nm. [b] Value for the dyes Eosin and Rhodamine-B measured in water.[234] [c] Time-averaged saturation intensity (intensity at which the fluorescence emission rate is half of its saturated value) from measurements using the mode-locked dye laser. [d] Derived from the measured transit time (1.8 ms) and the laser beam diameter.

collected following the release of the microsphere are also shown in Figure 8a. The inset in Figure 8a is an expanded view of the time axis near 0.5 s. A histogram of the burst sizes [total number of photoelectrons (pe) in a burst] from similar data is shown in Figure 8b. The peak at ~100 pe in the histogram is the result of single molecules passing through the center of the detection volume. Bursts >150 pe are caused by the presence of two or more analyte molecules in the detection volume. The probability of simultaneous occupancy of analyte molecules in the detection volume is a function of the burst detection rate and the transit time through the detection volume:[64]

$$P(2) = 1 - \exp(-R\tau_t) \qquad (4)$$

Here, $P(2)$ is the probability that two analyte molecules are in the probe volume at the same time, R is the detection rate, and τ_t is the transit time of an analyte molecule through the probe volume. Contributions from multiple occupancy can be reduced by time filtering the data as described above.[60] When a threshold is set at 45 pe, over 90% of the molecules are detected. At this threshold, there are few bursts from impurities dissolved in the sheath stream (false positives). The estimation of the detection efficiency was based on Monte Carlo calculations.[60] For the data shown in Figure 8, care was taken to ensure that all of the analyte molecules passed through the center of the detection volume where they received similar irradiation and experienced similar fluorescence detection efficiencies.

The importance of the analyte stream passing through the center of the detection volume is discussed by Goodwin[34] and Li.[17] If the sample stream is larger than the detection volume, most of the molecules are not detected and many pass through the edges of the detection region where the excitation rate is lower and the fluorescence photon collection efficiency is poor. This results in a burst size distribution that peaks at zero and decays monotonically. It is difficult to know where to set a threshold to distinguish molecules from background, and the detection efficiency is low.

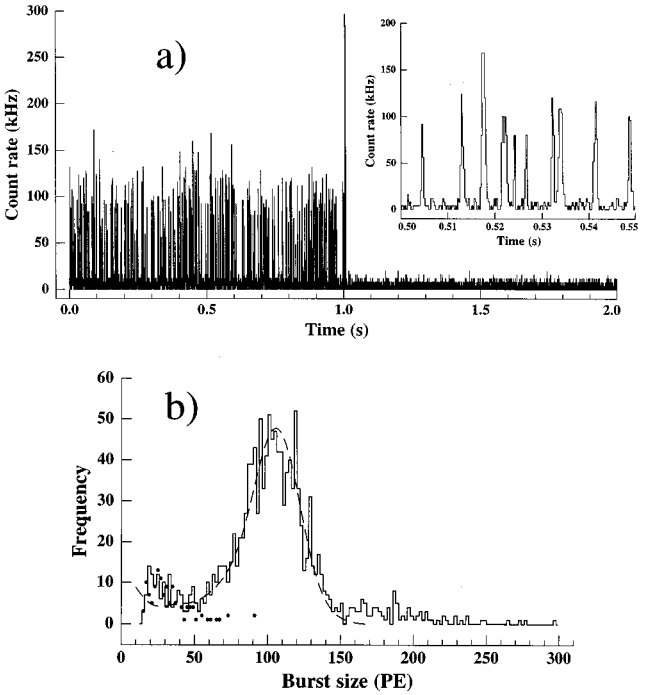

Figure 8. Time-gated TCSPC data showing fluorescence photon bursts from single R6G molecules desorbing from a dye-stained, 1 μm diameter microsphere optically trapped ~20 μm upstream of a 10 μm e^{-2} diameter excitation laser beam (panel a). At ~1 s the microsphere was released from the optical trap and flowed through the detection laser, as evidenced by the large (~300 kHz) photon burst. The inset shows an expanded view of the time axis near 0.5 s; photon bursts from single R6G molecules give peak photon counting rates of ~100 kHz. Panel b: time-filtered BSDs. A BSD compiled from data collected with a R6G stained microsphere held upstream of the detection volume is shown as a light, solid line. The peak at 100 photoelectrons (PE) is due to single R6G molecule fluorescence photon bursts; bursts greater than 150 PE are accidental coincidences (more than one R6G molecule in the detection volume simultaneously). The BSD shown with closed circles was compiled from data collected without a microsphere upstream of the detection volume; these bursts are due to fluorescent impurities in the sheath fluid. Each BSD was compiled from 55 s of data. The average R6G single molecule burst duration was 2.5 ms. To discriminate against background and accidental coincidences, only bursts with durations between 1 and 3.8 ms were included in the BSDs. The dashed curve is a BSD compiled from a Monte Carlo simulation of single R6G fluorescence bursts without accidental coincidences. Adapted from: Machara, N. P.; Goodwin, P. M.; Enderlein, J.; Semin, D. J.; Keller, R. A. *Bioimaging* **1998**, *6*, 33−42.

In a similar experiment, Li and Davis report the detection of Sulforhodamine 101 molecules injected into the sheath flow from a capillary with a submicrometer opening and constrained to pass through the center of the detection volume.[17] The probe laser was placed ~15 μm downstream from the capillary tip, and a sheath flow velocity of 1 cm/s was used to minimize diffusion of analyte molecules into the sheath stream. The authors report a detection efficiency of ~80% at a count rate of 150/s with most of the loss attributed to photodegradation.

Soper and co-workers demonstrated detection of single near-infrared fluorescent molecules.[10,65] Single molecules, dissolved in methanol, were excited at ~800 nm with the output from a mode-locked, Ti:

sapphire laser or a CW diode laser. Single molecule detection in the near-infrared benefits from reduced Raman scatter at longer wavelengths and fewer fluorescent impurity molecules that absorb in this wavelength region.

Diode laser-based detection of single molecules was also demonstrated by Sauer et al.[25] Derivatives of rhodamine dyes with large absorption coefficients, emission and absorption at wavelengths greater than 600 nm, fluorescence quantum yields >0.7, and good photostability were synthesized. These dyes were dissolved in ethylene glycol and excited with the output of a diode laser (632 nm). Fluorescence emission was detected with a SAPD (>60% efficiency at 670 nm). The authors report a background count rate <1 kHz and a signal-to-background ratio of 30−50 for the most intense bursts. Diode laser-excited, single molecule detection will become increasingly important because of its simplicity, small size, and low cost.

II.G.2. Identification at the Single Molecule Level

Different photophysical properties of fluorescent dyes have been used for identification at the single molecule level. Recent results are discussed in the following subsections.

II.G.2.a. Spectra. Soper et al. demonstrated the use of single molecule spectroscopy to distinguish between R6G and Texas Red.[66] R6G has a broad maximum in its absorption spectrum centered at ~530 nm and fluorescence emission peaked at ~550 nm. Texas Red absorbs at ~580 nm and emits at ~610 nm. A solution containing a mixture of the two dyes (5×10^{-14} M) was introduced into a flow cell. R6G molecules were excited by a frequency-doubled, mode-locked Nd:YAG laser (532 nm), and Texas Red molecules, by the output of a mode-locked dye laser tuned to 585 nm. The emission from the two dyes was separated by a dichroic beam splitter and focused onto different microchannel plate photomultiplier tubes. The data were processed by TCSPC as described above. The results are shown in Figure 9.

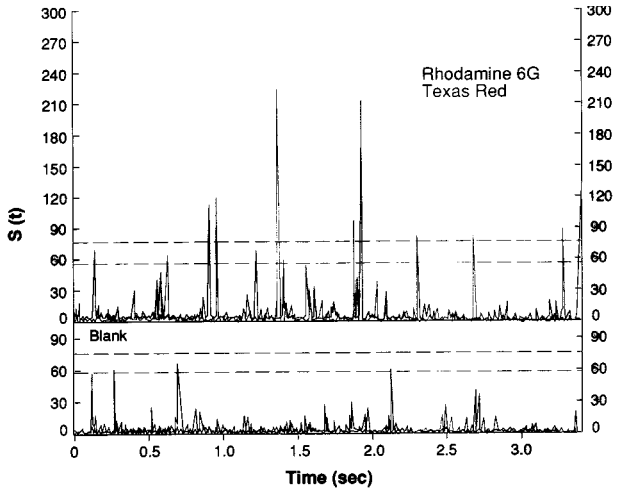

Figure 9. Distinguishing between R6G and Texas Red by their fluorescence spectra. The concentration of the dyes was 1×10^{-14} M in methanol. Discriminator thresholds were 86 for R6G and 65 for Texas Red. Reprinted with permission from: Soper, S. A.; Davis, L. M.; Shera, E. B. *J. Opt. Soc. Am. B* **1992**, *9*, 1761−1769. Copyright 1992 Optical Society of America.

Detected bursts were identified as due to either R6G or Texas Red with a high degree of confidence. This is a two laser, two detector technique. To our knowledge, this is the first demonstration of spectroscopy of single molecules in fluid solution.

Similar results were reported by Dörre et al., who distinguished between tetramethylrhodamine and Cy5 in a microchannel with two color irradiation and two color detection.[67]

II.G.2.b. Fluorescence Lifetime. With pulsed excitation and time-correlated detection, the arrival time of a detected photon with respect to the excitation pulse can be measured. A histogram of arrival times is a fluorescence decay curve and provides a measure of the fluorescence lifetime. This approach was used to measure the lifetimes of single molecules.[56,66] The fluorescence decay curve of a single molecule of Rhodamine-110 is shown in Figure 10.

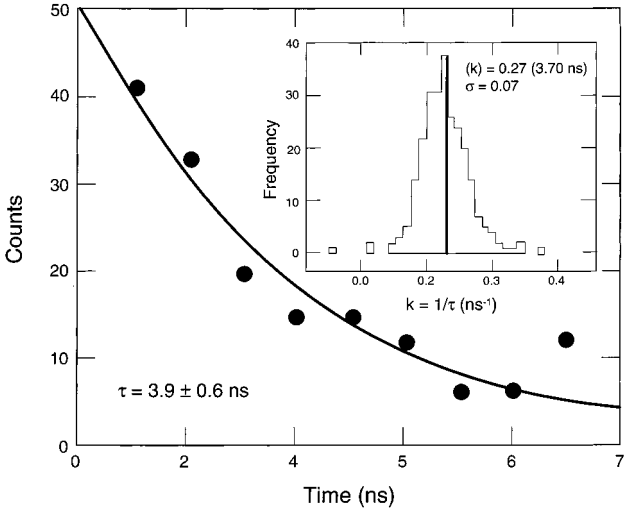

Figure 10. Fluorescence decay curve of a single molecule of Rhodamine 110. The solid line is an exponential decay derived from a maximum likelihood estimator. The inset shows the lifetime of several hundred Rhodamine 110 molecules determined at the single molecule level. The centroid corresponds to a lifetime of 3.7 ± 0.1 ns, in excellent agreement with a bulk measured lifetime of 3.8 ± 0.1 ns. Adapted from: Wilkerson, C. W., Jr.; Goodwin, P. M.; Ambrose, W. P.; Martin, J. C.; Keller, R. A. *Appl. Phys. Lett.* **1993**, *62*, 2030−2032.

Several groups have developed maximum likelihood methods to estimate the fluorescence lifetime from noisy data in a finite time window.[26,58,68−74] The fluorescence lifetime computed from the decay curve in Figure 10 using a maximum likelihood estimator is 3.9 ± 0.6 ns.[68] A histogram of the lifetimes of several hundred Rhodamine-110 molecules measured at the single molecule level is shown in the inset to Figure 10. The weighted mean decay rate of 0.272 ± 0.005 ns^{-1} corresponds to a fluorescence lifetime of 3.7 ± 0.1 ns, in excellent agreement with a bulk measured lifetime of 3.8 ± 0.1 ns. The width of the distribution is determined mostly by shot noise ($\sqrt{n}/n$) in the data.[68]

Single molecules can be identified by the measurement of their fluorescence lifetime.[26,74−79] This is an attractive approach because it requires only a single excitation laser and a single detection channel. The

accuracy of the extracted lifetime and the confidence of identification and distinguishing between different molecules is a function of the number of photons detected for each molecule and the differences in their fluorescence lifetimes.[70,78] A histogram of the fluorescence lifetimes of single molecules of an equimolar mixture of fluorescently labeled mononucleotides Cy5-dCTP ($\tau_f = 1.05 \pm 0.33$ ns), MR121-dUTP ($\tau_f = 2.07 \pm 0.59$ ns), and Bodipy-dUTP ($\tau_f = 3.88 \pm 1.71$ ns) dissolved in water is shown in Figure 11. Only

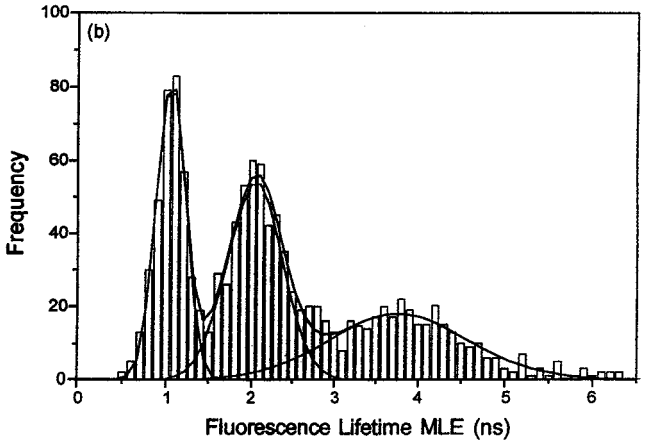

Figure 11. Distinguishing between Cy5-dCTP ($\tau_f = 1.05$ ns), MR121-dUTP ($\tau_f = 2.07$ ns), and Bodipy-dUTP ($\tau_f = 3.88$ ns), by their fluorescent lifetimes. Data are from a 10^{-11} M 1:1:1 mixture of the three components. Reprinted with permission from: Sauer, M.; Arden-Jacob, J.; Drexhage, K. H.; Göbel, F.; Lieberwirth, U.; Mühlegger, K.; Müller, R.; Wolfrum, J.; Zander, C. *Bioimaging* **1998**, *6*, 14−24. Copyright 1998 Institute of Physics Publishing.

bursts containing more than 30 pe were processed. The histogram shows three well-resolved peaks with the lifetime at each peak corresponding to one of the labeled nucleotides. From the overlap of the Gaussian fits to the peaks in the histogram, the authors estimate misclassification probabilities of 2% for Cy5-dCTP/MR121-dUTP and 7% for MR121-dUTP/Bodipy-dUTP. A solution containing a mixture of Cy5-dCTP and Bodipy-dUTP would have a misidentification probability of <1%. This technique was used to identify differently labeled antigen molecules in human serum.[77]

II.G.2.c. Burst Size. Van Orden et al. demonstrated the identification of single molecules by the size of the photon burst and a combination of the burst size and fluorescence lifetime.[79] Data for R6G are shown in Figure 12b, and that for a mixture of R6G and TRITC, in Figure 12a. Burst size distributions and intraburst fluorescence decay rates are projected onto the respective axes. The two parameter space is divided into four regions as shown in the figure. Bursts from R6G occur mostly in region II but extend into region III due to photobleaching in the laser beam resulting in bursts containing fewer photoelectrons. Bursts from TRITC occur almost completely in region I. For an equimolar sample of R6G and TRITC, 93% of the bursts in region I are due to TRITC and 99.8% of the bursts in region II are from R6G. Identification by burst size alone gives a 72% confidence for TRITC (region I + III) and a 98% confidence for R6G (region II + IV). Identification by intraburst decay rate alone gives a 90% confidence for TRITC (region I + IV) and 87% confidence for R6G (region I + III). The confidence levels reported here were derived from data simulation calculations described above, which gave an excellent reproduction of the observed distributions shown in Figure 12.

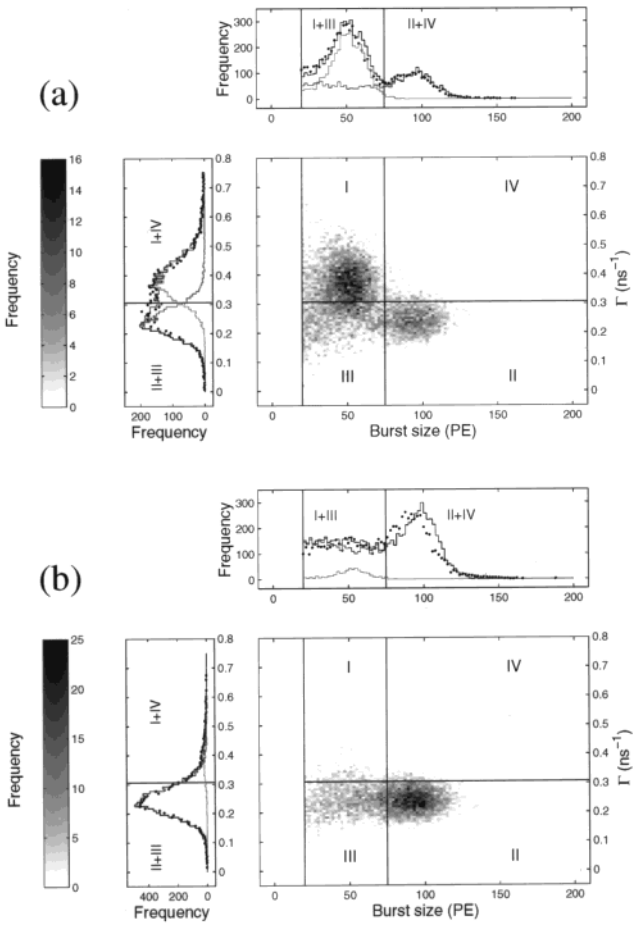

Figure 12. Correlated single molecule burst size and intraburst fluorescence decay rate measurements. The data are presented as two-dimensional histograms with darker shades of gray indicating increasing numbers of events. Key: (a) distribution compiled from data collected from a dilute sample stream containing approximately equal amounts of TRITC and R6G; (b) distribution compiled from data collected from a dilute sample stream containing mostly R6G. Projections of the correlated data onto the fluorescence decay rate and burst size axes are shown as solid circles to the left and above each scatter plot, respectively. Solid curves plotted on the projections are estimates, based on Monte Carlo simulations of the experiment. Analyte molecule introduction rates estimated from the simulations are ~20 TRITC s^{-1} and ~20 R6G s^{-1} in (a) and ~65 R6G s^{-1} and ~3 TRITC s^{-1} in (b). Reprinted from: Van Orden, A.; Machara, N. P.; Goodwin, P. M.; Keller, R. A. *Anal. Chem.* **1998**, *70*, 1444−1451. Copyright 1998 American Chemical Society.

II.G.2.d. Time-Resolved Fluorescence Anisotropy. Seidel et al. have demonstrated the use of time-resolved fluorescence anisotropy, which is related to the rotational relaxation time, to identify freely diffusing single molecules in solution.[80] Linearly polarized light was used to excite fluorescent molecules in solution. The parallel and perpendicular components of the fluorescence emission were analyzed by two different detectors. A mixture of Rhodamine 123

and Yellow Fluorescent Protein was studied. The two molecules have similar photophysical properties but rotational relaxation times that differ by 2 orders of magnitude. A histogram of the steady-state anisotropy of single molecules of the pure components and a mixture is shown in Figure 13. Rhodamine 123

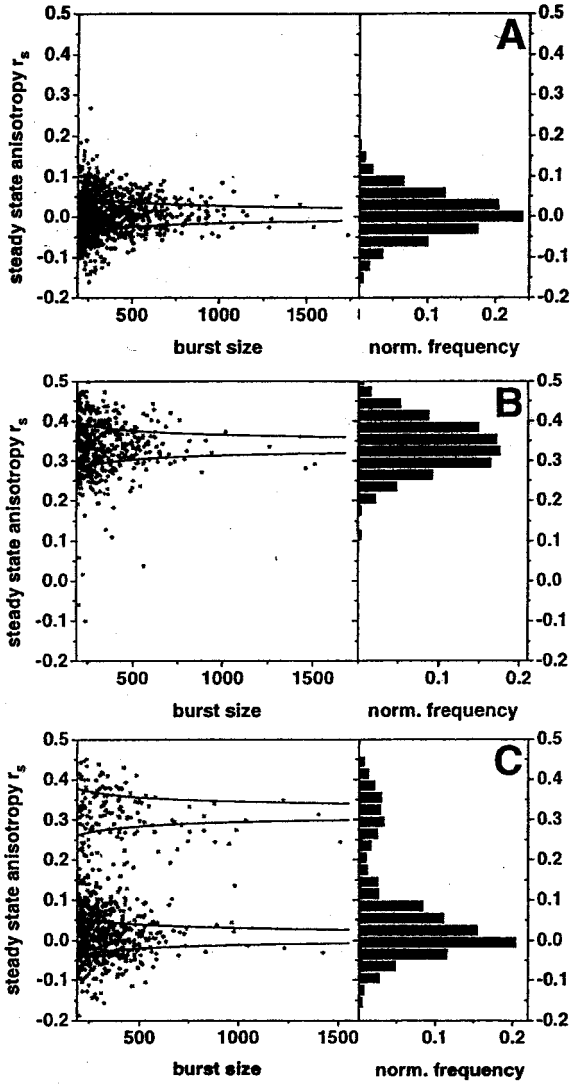

Figure 13. Distinguishing between Rhodamine 123 (A) and the Enhanced Yellow Fluorescent Protein (B) in mixture (C) by their steady-state anisotropies. Reprinted from: Schaffer, J.; Volkmer, A.; Eggeling, C.; Subramaniam, V.; Striker, G.; Seidel, C. A. M. *J. Phys. Chem. A* **1999**, *103*, 332−336. Copyright 1999 American Chemical Society.

rotates rapidly and has essentially zero steady-state anisotropy. Yellow Fluorescent Protein is much larger and has a steady-state anisotropy of ∼0.34. Two distinct bands with almost baseline resolution are observed for the mixture. Again, using the overlap of the Gaussian functions fit to the peaks in the histogram, the misclassification probability using steady-state anisotropy is ∼1%. Steady-state anisotropy measurements would be a good way of distinguishing between bound and free fluorescent probes. The authors suggest the use of multidimensional fluorescence spectroscopy (fluorescence lifetime, fluorescence anisotropy, and burst size) to reduce the misidentification probability for distinguishing between single molecules.

II.H. Applications

II.H.1. DNA Sequencing

Several groups are exploring a single molecule approach to DNA sequencing.[49,67,81−89] A *single* strand of DNA will be suspended in a flow stream and an exonuclease added to cleave sequentially the end nucleotide. Individual cleaved nucleotides released into the flow stream will be detected and identified by their fluorescence signature. This approach to DNA sequencing has the potential to sequence DNA at a rate of hundreds of bases per second. Even more important than the projected sequencing rate is the projected ability to sequence long fragments. Read lengths > 10 kilobases (10 kb) are anticipated, thereby reducing greatly the need of sequencing overlapping regions characteristic of the conventional sequencing process. In contrast to gel electrophoresis, this approach is not limited to 1000 base fragments or by current cloning bottlenecks. The proposed method of sequencing requires that only a single strand of DNA be anchored in the flow stream. Multiple strands cannot be used to increase signal because the distribution of enzymatic cleavage rates on the different DNA strands would result in the released nucleotides rapidly dephasing. Single molecule detection is required; to register the order there can be only one cleaved nucleotide in the detection region at any one time.

The fluorescence quantum yield of native nucleotides is low, and their spectral properties are similar. The detection of single native nucleotides has not been reported. Various strategies are being investigated to increase the fluorescence quantum yield of the nucleotides. Tagging the nucleotides with base-specific tags is an attractive approach.[49,66,67,81,82] DNA to be sequenced is denatured and replicated by polymerase primer extension with fluorescently tagged nucleotides. The fluorescently tagged nucleotides contain a highly fluorescent dye and a linker arm to separate the dye from the nucleotide. The linker arm is designed to prevent the tag from interfering with the polymerization and the exonuclease digestion. Strands of DNA several kilobases long with two or more of the nucleotide types fluorescently labeled have been prepared. DNA with all four nucleotide types labeled may be desirable, but the sequence can be determined from all combinations of two labeled nucleotide types.[85]

Fluorescent tagging of the nucleotides is time-consuming, and the fluorescent tags can potentially interfere with replication and digestion. An approach to identifying native nucleotides is to deposit the cleaved nucleotides onto a moving substrate and cool to low temperatures to increase the fluorescence quantum yield and improve the spectral resolution.[88] Postderivatization of the cleaved nucleotides to increase their fluorescence quantum yield is also under investigation.[88]

The detection of individual fluorescently labeled nucleotides cleaved from DNA attached to an optically trapped polystyrene microsphere suspended in an ultrasensitive flow apparatus is shown in Figure 14. Approximately 100 DNA fragments were attached

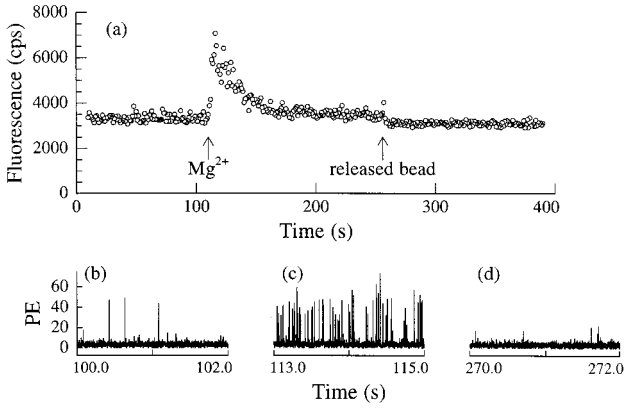

Figure 14. Detection of single, R6G-labeled nucleotides cleaved from fluorescently labeled DNA in flow. See text.

to the microsphere. Each fragment contained 40 bp with 8 of the last 22 bases being R6G-dUMP (Applied Biosystems, Inc.). Exonuclease III was present in the flow stream and was activated by the addition of Mg^{2+}. The flow stream was photobleached to reduce background from fluorescent impurities. The time-gated count rate is shown in Figure 14a. At ~100 s the Mg^{2+} reaches the microsphere and cleavage begins. The time-gated count rate increases abruptly and then falls as the DNA is digested. Exonuclease III cleaves fluorescently labeled DNA at a rate of ~1/s at 20 °C and ~5/s at 36 °C. At approximately 250 s, the bead is released and the time-gated count rate falls to the background rate. The scale is expanded in Figure 14b−d to show bursts from individual fluorescent molecules. Figure 14b shows bursts from fluorescent impurity molecules in the sheath and fluorescent molecules desorbing from the microsphere. Figure 14c shows bursts associated with individual fluorescent nucleotides cleaved from DNA on the microsphere, and Figure 14d shows bursts from impurity molecules in the sheath. Inspection of Figure 14b shows that bursts from impurity molecules from the sheath and microsphere (false positives) are approximately 2/s. The burst rate from a single fragment of DNA (~1/s) is similar to the background rate. Work is in progress to reduce the background and increase the cleavage rate.

Figure 15 shows the identification of single nucleotides cleaved from DNA by a combination of burst size and fluorescence lifetime (see section II.G.2.c).[89] In this case, the microsphere contained approximately 5000 45-mers with a single labeled R6G-dCTP near the 5′ end and a single tetramethylrhodamine-labeled dUTP near the 3′ end. Detected cleaved nucleotides were identified at a ~90% confidence level.

A German/Swedish consortium is exploring a similar approach to DNA sequencing.[67] A microsphere containing a single fragment of fluorescently labeled DNA will be optically trapped in a microchannel and digested by an exonuclease. Released tagged nucleotides, confined by the microchannel, will pass through a line of adjacent confocal detection volumes covering the cross section of the microchannel, where they will be detected and identified by a combination of their spectral characteristics and their fluorescent lifetimes.

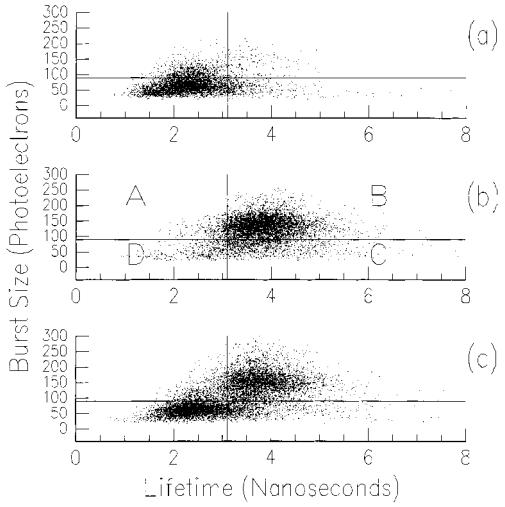

Figure 15. Scatter plots of burst size versus lifetime for three cleavage experiments. Top panel (a) shows ~4000 bursts detected during the cleavage of DNA labeled with TMR-dUMP. Middle panel (b) depicts ~5000 bursts detected during the cleavage of DNA labeled with R6G-dCMP. Bottom panel (c) shows ~8000 bursts detected during the cleavage of DNA labeled with one TMR-dUMP and one R6G-dCMP. The burst size/lifetime space has been divided into four quadrants, A−D. From the data in (a) and (b), we can assign the bursts in quadrant B as R6G-dCMP with 95% confidence and the bursts in quadrant D as TMR-dUMP with 90% confidence. Reprinted with permission from: Werner, J. H.; Cai, H.; Goodwin, P. M.; Keller, R. A. *Proc. SPIE* **1999**, *3602*, 355−366. Copyright 1999 International Society for Optical Engineering.

II.H.2. DNA Fragment Sizing

The sizing of DNA fragments created by a restriction digest is an important analytical tool in medical diagnostics and forensics. A DNA sample is digested with a restriction enzyme that cuts at a sequence characteristic of that restriction enzyme. The length of specific fragments is characteristic of a particular individual and is used for forensic identification. The length of other fragments can be indicative of the presence of a gene responsible for a serious disease. Restriction fragment length distributions are customarily analyzed by gel electrophoresis. The analysis requires nanograms to micrograms of material and takes tens of hours.

A flow cytometric single molecule detection technique can be used to size DNA fragments.[90−97] Flow cytometric sizing of DNA fragments is the subject of a recent review.[98] A restriction digest of a DNA sample is stained with an intercalating dye that reacts stoichiometrically with the DNA; the amount of dye intercalated is directly proportional to the fragment length (number of base pairs). Commonly used intercalating dyes have fluorescence enhancements of several orders of magnitude upon binding to DNA[99] making it unnecessary to remove unbound dye before the analysis. The stained fragments are diluted to $\sim 10^{-14}$ M and passed individually through an ultrasensitive flow cytometer. The intensity of the fluorescence from each fragment (burst size) is a measure of the fragment length. At our flow rates (~2 cm/s) DNA fragments larger than ~10 kbp are stretched out and aligned parallel to the flow axis. Intercalated dye molecules are then aligned

with their transition dipoles perpendicular to the flow axis. Care must be taken to avoid polarization effects in excitation and detection.[100] For our geometry, polarization effects are small and are ignored.

A histogram of the burst sizes from a mixture of λ DNA and a Hind III digest of λ DNA is shown in Figure 16. This plot is the result of analyzing ~3 min

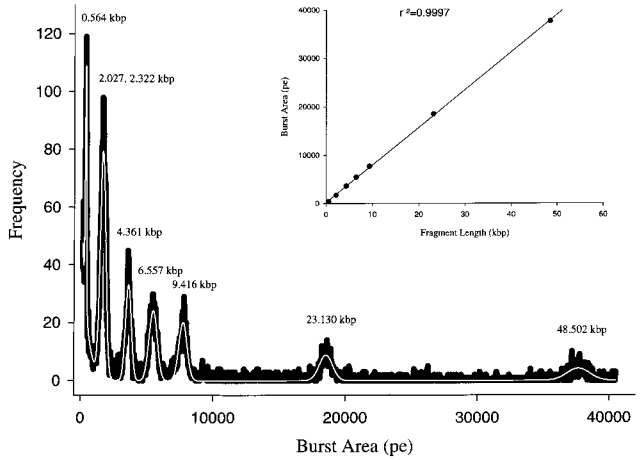

Figure 16. Hind III restriction digest of λ DNA stained with POPO-3. Seven peaks are well resolved. The inset is a plot of the centroids of the peaks vs the known fragment lengths.

of data containing measurements of ~10 000 DNA fragments (<1 pg of DNA). Peaks corresponding to the fragment sizes 23.130 kbp, 9.416 kbp, 6.557 kbp, 4.361 kbp, and 0.564 kbp are well resolved. The doublet at ~2.0 kbp is not resolved. The data were fit to a sum of seven Guassians and an exponential background. (An exponential function was found empirically to be a good representation of the background.) The centroids of the peaks determined from the fit are plotted verses the known fragment sizes in the inset. A linear least-squares fit is also shown in the plot. The correlation coefficient of the fit is 0.9997. No point deviates from the fit by as much as 2%. Since the sizes of λ DNA and the fragments in its digest are known exactly from sequence data, Figure 16 is a good measure of the accuracy of the flow cytometric approach to DNA sizing. For comparison, a similar sample was analyzed by conventional gel electrophoresis. The gel was loaded with 200 ng of DNA and run for 22 h. The resolution by gel electrophoresis is better for small fragments. At ~10 kbp the resolution for the two approaches is similar, and above 10 kbp the resolution for the flow cytometric approach is better. The flow cytometric approach is more of a competitor to pulsed-field gel electrophoresis (PFGE) commonly used for the sizing of DNA fragments larger than 30 kbp. The smallest fragment sized successfully by flow cytometry is 245 bp.[96]

λ DNA has a complementary, 12 base overhang at each end (sticky ends). These overhangs can hybridize to form concatamers. Figure 17 shows a histogram of flow cytometric sizing of a sample containing concatamers of λ DNA.[95] Fragments containing up to 7 units of λ DNA are visible. The fragment containing 7 units has a length of 395 kbp. Also shown in Figure 17 is a plot of the centroids, extracted from

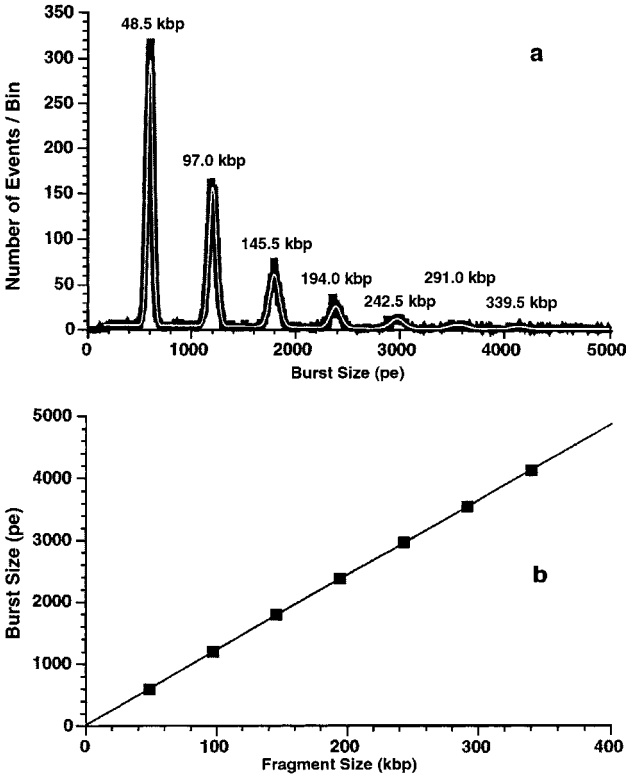

Figure 17. Sizing of λ DNA concatamers: (a) histogram of the fluorescent burst sizes of λ DNA concatamers stained with TOTO-1; (b) plot of the burst size means from a Gaussian fit to the data in (a). The correlation coefficient of the linear fit is 0.999 98. Reprinted with permission from: Huang, Z.; Jett, J. H.; Keller, R. A. *Cytometry* **1999**, *35*, 169−175. Copyright 1999 Wiley.

a fit to the histogram, versus the known fragment lengths. The fit is linear with a correlation coefficient of 0.999 98. The maximum deviation from the fitted line is 1.8%. Again, because the sequence of λ DNA is known, this is a good measure of the accuracy of flow cytometric DNA sizing.

PFGE is routinely used to identify bacteria by the analysis of a restriction digest of the bacteria's genome. Flow cytometric fragment sizing can also be used to identify bacteria species and strain.[95,97] Histograms of a Not I digest of *Escherichia coli*, *Bacillus globigii*, and *Escherichia herbicola* are shown in Figure 18. The fingerprints are clearly different and form a basis for identification. The centroids of the fit to the histograms plotted against the fragment lengths determined by PFGE are also shown in Figure 18. The plots are linear with correlation coefficients > 0.98. Deviations of the points from the fit line are larger than those in Figure 17. This is attributed to the inherent 10% inaccuracy associated with DNA fragment sizing by PFGE.

An initial step in conventional DNA sequencing is the preparation of DNA libraries. Chromosomes, sorted by flow cytometry or other sources of DNA, are digested by a restriction enzyme and hybridized to a cloning vector. The vector plus insert are injected into a bacterium where it is replicated by the bacterium. The cloned DNA (PAC clone) is extracted from the bacterium for sequencing or other analyses. Typically, the fragments produced are characterized by PFGE to determine the validity of the cloning

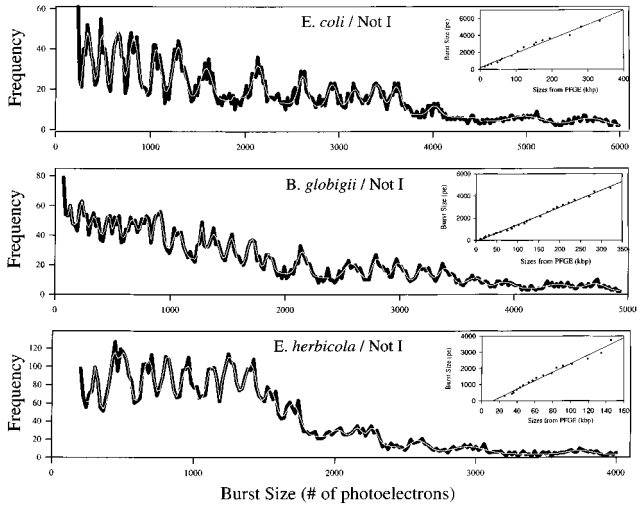

Figure 18. Histograms of the burst sizes for the Not I digestion of *E. coli*, *B. globigii*, *and E. herbicola* stained with TOTO-1. The solid line represents the raw data, and the white line represents the Gaussian fit. The insets are plots of the extracted centroids vs the fragment lengths from PFGE. Reprinted with permission from: Kim, Y.; Jett, J. H.; Larson, E. J.; Penttila, J. R.; Marrone, B. L.; Keller, R. A. *Cytometry* **1999**, *36*, 1−9. Copyright 1999 Wiley.

process. PAC clones can be sized by flow cytometry.[94] Intact PAC clones were isolated from *E. coli* using a rapid alkaline lysis miniprep method[101] and sized by flow cytometry. Histograms of four PAC clones plus DNA standards (λ KpnI digest, λ DNA, and T4 DNA) are shown in Figure 19. The histograms are the result of analyzing ~3 min of data obtained from ~5000 DNA fragments (<1 pg of DNA). The clone sizes extracted from a fit to the data are compared to PFGE results in Table 2. The flow cytometry numbers in the table are calculated by subtracting the vector size (15.9 kbp). The two approaches agree within the 10% uncertainty associated with PFGE.

Table 2. Comparison of the Sizes of Clones from a PAC Library Measured by Flow Cytometry and Pulsed-Field Gel Electrophoresis

clone	flow cytometry (kbp)	PFGE (kbp)
A	89.1 ± 1.7	97 ± 10
B	85.8 ± 1.8	93 ± 9
C	79.6 ± 0.9	81 ± 8
D	87.3 ± 1.9	94 ± 9

II.H.3. Two Color Homogeneous Assay for Probe/Target Binding

The determination of binding of a probe molecule to a target molecule is a common assay in biochemical analysis. Typically, the probe molecule is labeled with a fluorescent tag and fluorescence from the probe/target complex is used to signal the binding. In most cases, the unbound probe must be separated from the solution before the assay so that the measured fluorescence comes only from the complex (heterogeneous assay). This assay can be done at the single molecule level without separation of the unbound probe from the solution by using two color detection (homogeneous assay). The probe is labeled with one color, and the target, with another color. The presence of a single species containing both colors is indicative of binding.

This approach has been used to detect specific nucleic acid sequences in unamplified genomic DNA.[102] Two nucleic acid probes complementary to different sites on a target DNA were labeled with different fluorescent dyes (R6G and Bodipy TR). The labeled probes were mixed with a DNA sample and allowed to hybridize. Binding of both probes to the target DNA is indicated by a single species containing both tags. Figure 20 shows the detection of phage λ DNA in a background of salmon DNA at a relative concentration of one λ DNA/salmon genome. Two coincidences were detected in 8 s of data. The authors

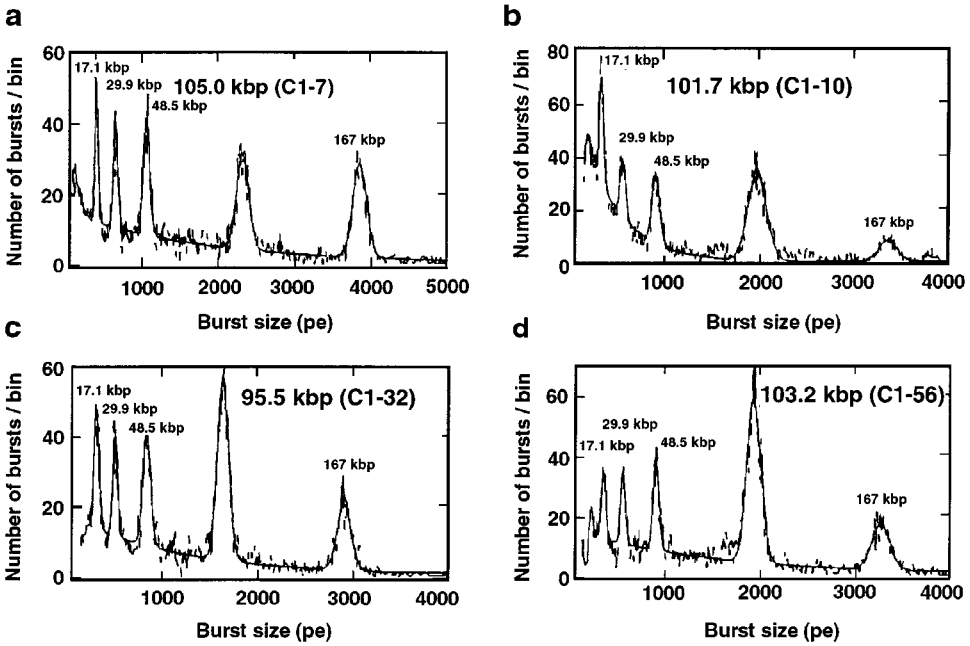

Figure 19. Histograms of the fluorescence burst sizes of clones from a PAC clone library. λ *Kpn*I digest, λ DNA, and T4 DNA were used as markers. The DNA was stained with TOTO-1. The clone sizes obtained from a linear fit to the markers are listed. Reprinted with permission from: Huang, Z.; Petty, J. T.; O'Quinn, B.; Longmire, J. L.; Brown, N. C.; Jett, J. H.; Keller, R. A. *Nucleic Acids Res.* **1996**, *24*, 4202−4209. Copyright 1996 Oxford University Press.

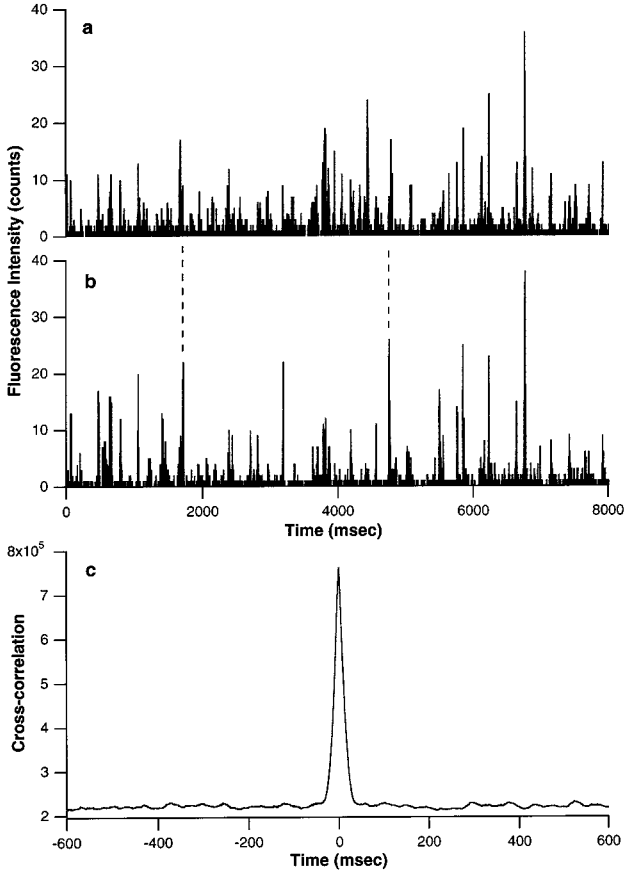

Figure 20. Detection of λ DNA in a sample containing an excess of salmon genomic DNA and two fluorescent probes complementary to two sequences on λ DNA. One probe is labeled with R6G, and the other, with Bodipy-TR. Fluorescence was detected with two detectors—one tuned to R6G and the other to Bodipy-TR. Most of the bursts shown in (a) and (b) are from unbound probes present in the solution. Cross-correlation of the signal from the two detectors identifies bursts from both probes on the same DNA fragment. Two such bursts are indicated by the dashed lines. Reprinted from: Castro, A.; Williams, J. G. K. *Anal. Chem.* **1997**, *69*, 3915−3920. Copyright 1997 American Chemical Society.

also report the detection of a single copy BT transgene in a maize genomic sample.

II.H.4. Single Molecule Electrophoresis

Single molecule detection with confocal optics was applied to capillary electrophoresis.[103,104] A laser beam was focused to a 2 μm diameter in the center of a 100 μm, gel-filled capillary tube containing a mixture of pBR 322 DNA (4.6 kbp) and pRL 277 DNA (6.8 kbp) intercalated with a thiazole orange derivative. Application of an electric field caused the sample to separate because of the different electrophoretic mobilities of the two DNAs. The electrophoretagram is shown in Figure 21. Two distinct clusters of single molecule photon bursts were observed. Because only a small cross section of the capillary was irradiated, the detection efficiency was ~0.1%.

Fister et al. report the electrophoretic separation of R6G and Rhodamine B in a glass microchannel of dimensions 10 μm deep, 48 μm wide at the top, and 32 μm wide at the bottom.[105] Confocal techniques were used resulting in a detection efficiency of 1.75%.

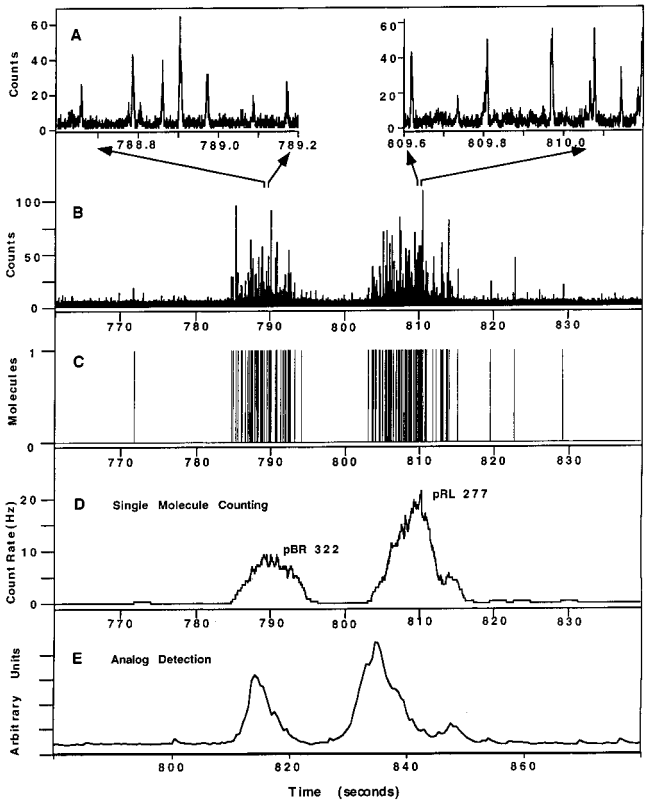

Figure 21. Capillary gel electrophoresis with single molecule detection. pBR 322 DNA (4.6 kbp) was separated from pRL 277 DNA (6.7 kbp). The DNA was stained with the fluorescent intercalating dye TO6. Fluorescence bursts from individual DNA fragments are shown in panel A. A total of 80 s of raw data showing burst in both DNA bands is shown in panel B. Counts of single molecules are shown in panel C. A histogram of single molecule counts is shown in panel D. Analogue detection is shown in panel E. Reprinted from: Haab, B. B.; Mathies, R. A. *Anal. Chem.* **1995**, *67*, 3253−3260. Copyright 1995 American Chemical Society.

This paper contains an excellent description of optimum data analysis, errors, reentry effects, and problems associated with single molecule electrophoresis. Concentration detection limits at the >99% confidence level were reported as the following: 1.7 pM, R6G; 8.5 pM, Rhodamine B.

A novel method to measure electrophoretic mobilities was developed by Castro et al.[18] A schematic of the apparatus is shown in Figure 22. An electric field is applied along a square-bore flow cell. Two tightly focused, parallel laser beams displaced by 250 μm intersect the flow cell perpendicular to the flow axis. The electrophoretic velocities of individual molecules in a mixture are measured by the time it takes the molecule to travel between the two laser beams. Typical migration times are ~500 ms. In some cases, a dilute solution of a low-viscosity, entangled polymer was added to increase the differences in electrophoretic mobility between analyte molecules. This technique was used to size a restriction digest of λ DNA and analyze a mixture of proteins. Note that this is a continuous analysis process, as opposed to a batch process characteristic of conventional electrophoresis, and is applicable for the continuous monitoring of sample streams.

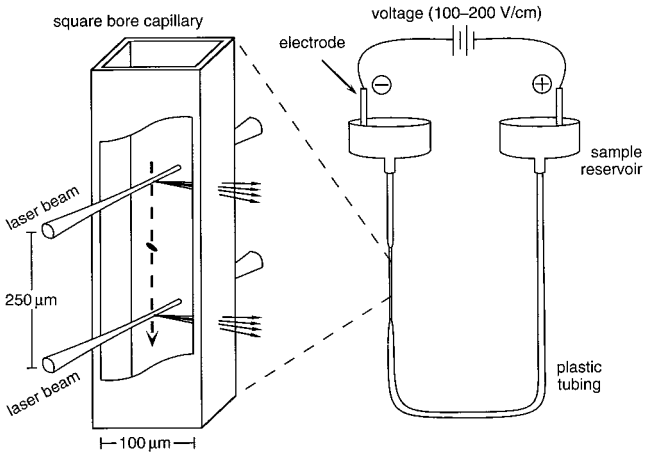

Figure 22. Single molecule electrophoresis apparatus. An expanded view of the flow cell showing the two parallel laser beams passing through the cell is shown at the left. Fluorescence light is represented by two sets of arrows. Reprinted from: Castro, A.; Shera, E. B. *Anal. Chem.* **1995**, *67*, 3181−3186. Copyright 1995 American Chemical Society.

III. Single Molecule Spectroscopy on Levitated Microdroplets

Another successful approach to single molecule detection in liquids is laser-induced fluorescence detection of single fluorescent molecules dissolved in levitated[6,106,107] and falling[108−111] microdroplets. The major advantages of this approach are the small detection volumes afforded by micrometer size droplets (1 μm diameter is equivalent to 0.5 fL) and the confinement of the analyte molecule in the microdroplet. Small microdroplet volumes minimize background emission due to solvent Raman and Rayleigh scattering and impurity fluorescence. Confinement of the analyte in a levitated microdroplet allows it to be illuminated for times sufficiently long to photolyze the analyte molecule, thereby allowing the maximum number of fluorescence photons to be extracted from the molecule. Complications arise due to position-dependent variations of the excitation laser intensity and fluorescence emission collection efficiency inside of the microdroplet caused by refraction of incident excitation and emitted fluorescence at the microdroplet surface. Both effects reduce the detection efficiency for analyte molecules located in certain regions of the microdroplet.[112,113] This can be alleviated to some degree by using a counterpropagating-beam excitation geometry and saturating the absorption of the analyte. Moreover, small movements of the microdroplet with respect to the counterpropagating excitation laser beams as well as rotation of the microdroplet and diffusion of the analyte within the microdroplet improve the uniformity of the time-averaged excitation and fluorescence emission collection efficiencies experienced by an analyte molecule.[112,113]

Initial experiments with electrodynamically levitated ∼10 μm diameter (∼1 pL volume) glycerol−water droplets using CW argon ion (514 nm) laser excitation and only modestly efficient fluorescence emission collection optics demonstrated detection limits of ∼10 molecules for R6G[106] and a single molecule for B-phycoerythrin[107] (a fluorescent protein containing 34 chromophores with a fluorescence yield equivalent to ∼25 R6G molecules). Subsequent experiments on smaller (4 μm diameter, ∼35 fL) levitated microdroplets using higher efficiency fluorescence emission collection optics demonstrated the detection of single R6G molecules with signal-to-noise ratios from 25 to 45.[6]

A major drawback of sensitive detection in levitated microdroplets is the extremely low sample throughput rate. Typically, for the work with levitated droplets described above, several minutes were required to trap and measure one microdroplet.[31] High sensitivity and increased throughput were demonstrated using a stream of microdroplets falling, one-at-a-time, through a CW excitation laser. Early work by Mahoney et al. demonstrated a detection limit of ∼8 amol of R6G dissolved in 225 μm diameter (6 nL) ethanol microdroplets falling through a low intensity (250 W/cm^2) Ar^+ (514 nm) laser beam at a throughput of 150 droplets/s.[108] Ramsey and coworkers subsequently demonstrated detection of single R6G molecules dissolved in an electrodynamically focused stream of ∼7 μm diameter (∼150 fL) glycerol−water microdroplets falling through the 90 μm waist of a counter-propagating Ar^+ (514 nm) laser at a rate of 2−5 droplets/s.[109,110] Figure 23 shows a schematic of this experimental setup. A linear electric quadrupole was used to focus the falling droplet stream through the center of the excitation laser beam waist. Single molecule sensitivity was achieved through a combination of small sample volume, high

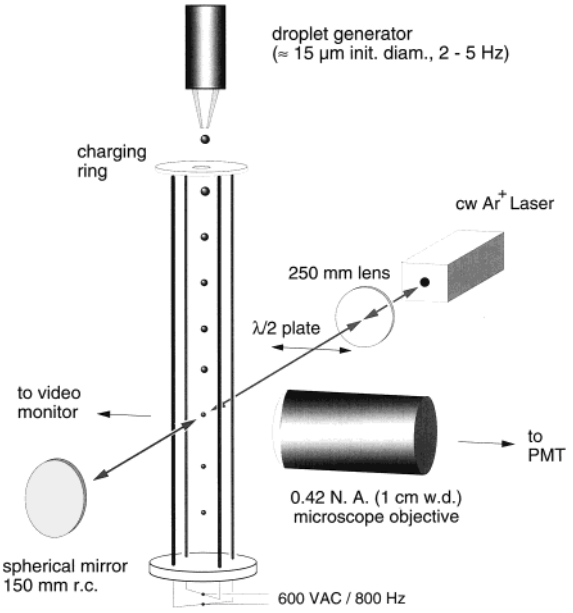

Figure 23. Schematic of an experimental setup to detect single molecules dissolved in a stream of free-falling microdroplets. A linear quadrupole focuses the falling droplet stream through the 90 μm e^{-2} diameter waist of a retroreflected CW Ar^+ laser beam. The initial diameter of the microdroplets was ∼15 μm; by the time they reached the detection region the diameter was reduced, by water evaporation, to 7 μm. Legend: r.c., radius of curvature; VAC, ac volts; w.d., working distance. Reprinted with permission from: Barnes, M. D.; Lermer, N.; Kung, C.-Y.; Whitten, W. B.; Ramsey, J. M.; Hill, S. C. *Opt. Lett.* **1997**, *22*, 1265−1267. Copyright 1997 Optical Society of America.

fluorescence emission photon collection and detection efficiencies, efficient scattered light rejection, and high (~50 kW/cm^2) excitation intensity. A molecule detection efficiency of ~80%, limited primarily by the photostability of R6G, was reported. Figure 24 shows

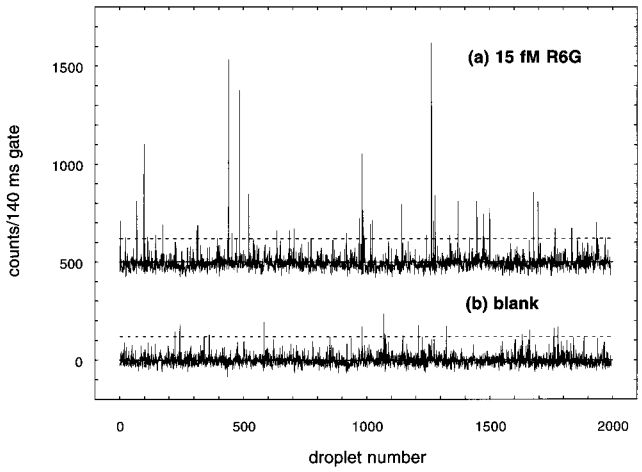

Figure 24. Detection of single R6G molecules dissolved in free-falling glycerol−water microdroplets: (a) 2000-droplet run generated from a 15 fM R6G water−glycerol solution (offset by 500 counts for clarity); (b) 2000-droplet run generated from a blank solution. The average blank signal of 340 counts has been subtracted from both runs. A 3-σ detection threshold (120 counts above the mean) is indicated with dashed lines. Reprinted with permission from: Barnes, M. D.; Lermer, N.; Kung, C.-Y.; Whitten, W. B.; Ramsey, J. M.; Hill, S. C. *Opt. Lett.* **1997**, *22*, 1265−1267. Copyright 1997 Optical Society of America.

results from a 15 fM solution of R6G and a blank.

Very recently, Ramsey and co-workers reported the detection of single R6G molecules dissolved in 1 μm diameter water droplets falling through the 25 μm waist of an argon-ion laser beam.[111] Under these conditions, the analyte was confined to 0.5 fL, a volume comparable to those obtained with diffraction-limited, confocal microscopy techniques. Since the R6G molecules were confined to the microdroplets, sample illumination times as long as 20 ms were used, more than 1 order of magnitude longer than the diffusion-limited residence time of a R6G molecule in an open 0.5 fL volume in aqueous solution.

An emerging application of single molecule spectroscopy in microdroplets is the study of single molecule microcavity effects. Recently, Lermer et al. demonstrated detection of individual, spatially photoselected octadecyl Rhodamine B (ODRB, a surfactant) molecules localized on the surfaces of microdroplets.[114] They observed excitation laser polarization dependent photon statistics for single ODRB molecules that were not observed for single Rhodamine B molecules that take random positions and orientations anywhere within the microdroplet.

IV. Confocal Excitation and Detection for Single Molecule Spectroscopy

IV.A. Single Molecule Detection

Confocal excitation and detection can be used to attain subfemtoliter probe volumes. With these small volumes, background emission from the solvent is negligible and single molecules have been detected with large signal-to-noise ratios. In confocal microscopy, the excitation laser is reflected from a dichroic beam splitter and focused by a microscope objective to a ~1 μm diameter waist in the sample. Fluorescence from the sample is collected by the same microscope objective, passed by the dichroic beam splitter, and focused onto a pinhole (~50 μm in diameter). Light transmitted through the pinhole is imaged onto a photon detector. Emission from analyte molecules outside of the image of the pinhole in the sample is out of focus and does not pass through the pinhole. The probe volume (typically ~1 fL) is determined by the image of the pinhole in the sample and the spherical aberration of the microscope objective. A schematic of a confocal microscope is shown in Figure 25. Single molecules are detected as they

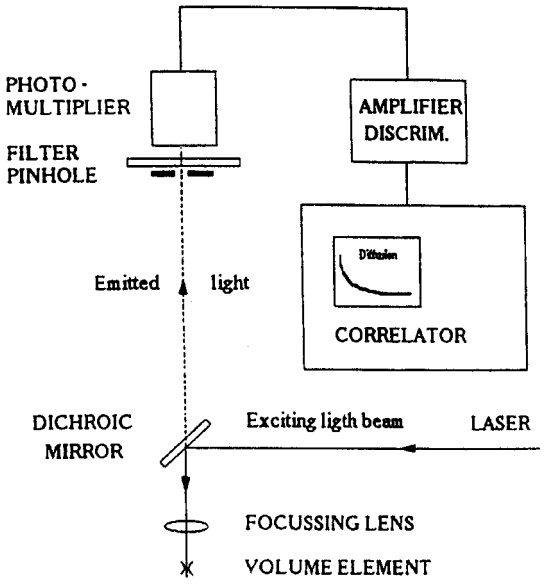

Figure 25. Setup for confocal fluorescence measurements. The excitation laser reflects off a dichroic mirror and is focused by a lens (a high NA microscope objective) to a diffraction limited spot in the sample. Fluorescence emitted from molecules in this volume is imaged by the same lens used to focus the laser. This fluorescence passes through the dichroic mirror and through a pinhole in the image plane of the objective. A cutoff filter blocks much of the scattered light generated by the excitation laser. A photomultiplier is used to detect the collected fluorescence; this signal is amplified by a discriminator, and the output is autocorrelated (see section IV.B). Reprinted with permission from: Rigler, R.; Widengren, J.; Mets, Ü. In *Fluorescence Spectroscopy*; Wolfbeis, O. S., Ed.; Springer-Verlag: Berlin, 1993. Copyright 1993 Springer-Verlag.

diffuse through the probe volume. The diffusion time of an analyte molecule through a femtoliter probe volume is approximately 1 ms. At 10^{-12} M, the instantaneous probability that a femtoliter probe volume contains an analyte molecule is ~0.001. Autocorrelation analysis of the data is informative but not necessary to detect single molecules by confocal microscopy.

The use of confocal techniques to detect single molecules was pioneered by Rigler and co-workers.[9,84,115,116] Photon bursts from single R6G molecules in water diffusing through a 0.24 fL probe volume

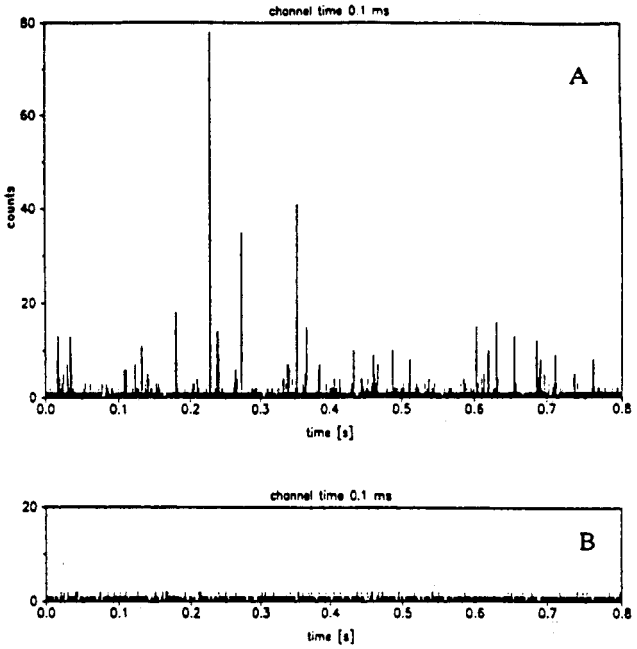

Figure 26. Detection of single molecules of R6G in water by confocal fluorescence microscopy: panel A, 2×10^{-12} M R6G; panel B, pure water. Reprinted with permission from: Mets, Ü.; Rigler, R. *J. Fluoresc.* **1994**, *4*, 259−264. Copyright 1994 Kluwer Academic.

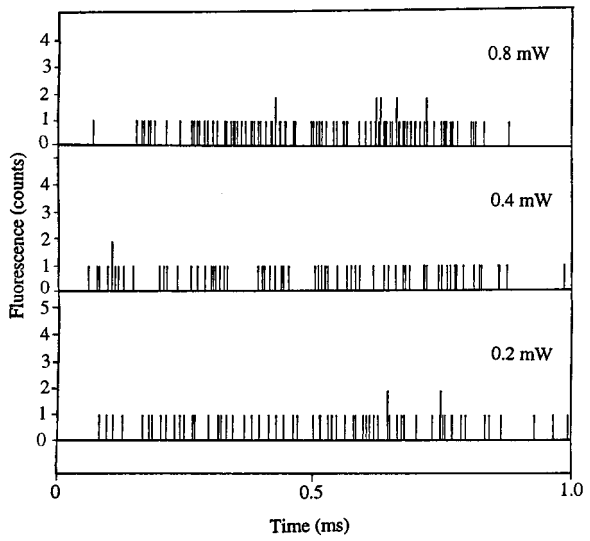

Figure 27. Time records of fluorescence emission of single R6G molecules at different laser powers. Reprinted with permission from: Nie, S.; Chiu, D. T.; Zare, R. N. *Science* **1994**, *266*, 1018−1021. Copyright 1994 American Association for the Advancement of Science.

are shown in Figure 26. The authors report a signal-to-background ratio of 1000; in some cases, only 4 recorded photoelectrons were needed to detect a molecule. Similar results were reported by Nie et al.[14,117] Data streams for the detection of single molecules of R6G at different excitation powers are shown in Figure 27. Each panel shows the time distribution of detected photoelectrons as a single molecule diffuses through the probe volume. Short gaps in the data are attributed to intersystem crossing into the metastable triplet state (lifetime ~4 μs), and the longer gaps (~50 μs), to the same molecule diffusing in and out of the probe volume. The same molecule reentering the probe volume several times results in an overestimation of the concentration when counting single molecules. Chiu et al. observed the same phenomena with 14 nm fluorescent microspheres.[118] Thirty-five percent of the spheres reentered the probe volume in good agreement with theoretical estimates. In addition, they observed effects attributable to optical trapping—microspheres remained in the probe volume longer than is predicted by molecular diffusion. The authors also demonstrated optical trapping and manipulation of YOYO-stained λ DNA and several fluorescently labeled proteins.

As reported above, confocal excitation with diode lasers has been used to detect and identify single molecules in solution.[26,75−78]

Generally, the molecule detection efficiency in confocal spectroscopy is extremely low because it is difficult to make the analyte molecules pass through such a small probe volume. Histograms of observed burst sizes peak at zero and decay monotonically. (See discussion of detection efficiency in section II.G.1). For applications where efficient detection of the analyte is required, it is best to choose the largest probe volume consistent with an acceptable signal-to-noise ratio for the application under study. Recently, the use of microcapillaries and microstructures to force the molecules to pass through the detection volume has resulted in larger molecule detection efficiencies for confocal microscopy (see section V).

An interesting application of single molecule detection with confocal microscopy is the observation of the dynamics of a single dye molecule interacting with guanine on a DNA strand.[119−122] Edman et al. report two conformations for tetramethylrhodamine tethered to a short DNA oligomer.[119,120,122] Eggeling et al. studied the same system and attributed their results to three conformations: (1) the tethered dye stretched out in solution ($\tau_f = 2.2$ ns); (2) the dye in the hydrophobic environment of the DNA ($\tau_f = 3.7$ ns); (3) the dye complexed to guanine where its fluorescence was quenched by electron transfer to the guanine ($\tau_f = 1.3$ ns).[121] These confirmations were characterized by their fluorescence lifetime and burst size. The average dwell time of a single molecule in each state was reported as the following: (1) 6.7 ms; (2) 5.1 ms; (3) 3.1 ms.

IV.B. Fluorescence Correlation Spectroscopy in Liquids

In general, the amount of light emitted from a probe volume is proportional to the number of fluorescent molecules present in the volume. Fluorescence correlation spectroscopy (FCS) makes use of the fact that the number of fluorescent particles present in a given volume fluctuates in time, due to diffusion into and out of the volume or via a transition of the molecules between fluorescent and nonfluorescent states while inside the volume[123,124] (see Figure 28). The FCS technique uses an autocorrelation of the light intensity emitted from the volume. The normalized autocorrelation function

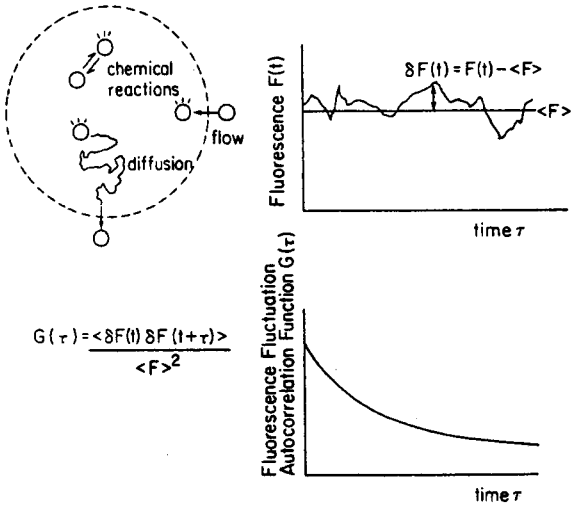

Figure 28. Schematic diagram that illustrates the conceptual basis for FCS experiments. Top left: The number of fluorescent species in an illuminated probe volume can change by diffusion of molecules into the volume or by a chemical reaction inside the volume that creates a fluorescent product. Top right: These fluctuations in the number of fluorescent species in the volume generate changes in the emitted light intensity. Bottom: The deviations in light intensity from the average are autocorrelated. The time scale of the decay and the amplitude of the autocorrelation function reveal useful kinetic information (see text). Reprinted with permission from: Thompson, N. L. In *Topics in Fluorescence Spectroscopy*; Lakowicz, J. R. Ed.; Plenum Press: New York, 1991; Vol. 1, pp 337−378. Copyright 1991 Plenum Press.

is given by[124]

$$G(\tau) = \frac{\langle \delta F(t+\tau)\delta F(t)\rangle}{\langle F(t)\rangle^2} \qquad (5)$$

where the brackets $\langle\ \rangle$ indicate an average over time t, $F(t)$ denotes the fluorescence intensity at time t, and $\delta F(t)$ is the deviation of the fluorescence intensity from the average (i.e. $\delta F(t) = F(t) - \langle F\rangle$). The amplitude of the autocorrelation function is inversely proportional to the number of molecules in the volume, and the temporal decay of the autocorrelation function is indicative of the time scale of the fluctuations.[123,124] In FCS, fluctuations in light intensity are relatively larger for a small number of fluorescent molecules present in the probe volume. This makes FCS an ideal technique for detecting a small number of molecules, with the ultimate detection limit of a single fluorophore in the probe volume at any one time.[123]

The theory of FCS for chemically reacting systems and translational diffusion was first developed by Magde, Elson, and Webb in the early 70's, who used FCS to study the binding of ethidium bromide to DNA.[125] This group and others later extended FCS to measure rotational diffusion.[126−129] Other early efforts applied FCS to the study of translational diffusion,[125] reversible isomerization,[130] and bimolecular chemical reactions.[130]

A major advantage of FCS is the ability to make measurements on an inhomogeneous system without separation of the components. An early example was the development of an FCS immunoassay that did not require the separation of bound targets from unbound reporter dye.[131] More recently, FCS was used to investigate ligand−receptor binding kinetics.[132] Another recent application used FCS to measure the electrophoretic mobilities of molecules.[133] The bound probes can be distinguished from the unbound probes by their different electrophoretic mobilities. This technique has the advantage that probe−target binding can be detected even if the combined probe−target has a diffusion constant and fluorescence quantum yield similar to those of the unbound probe. More emerging applications of FCS may be found in recent reviews.[123,124,134]

Subfemtoliter probe volumes provide excellent background suppression and have allowed many FCS studies to be performed on samples at the single molecule level.[9,67,84,115,135−155] Rigler and Mets were the first to perform FCS under conditions where the average number of molecules in the probe volume was less than 1.[115] Figure 29 shows an autocorrelation function where the average number of fluorescent molecules in a 0.2 fL probe volume was only 0.005.

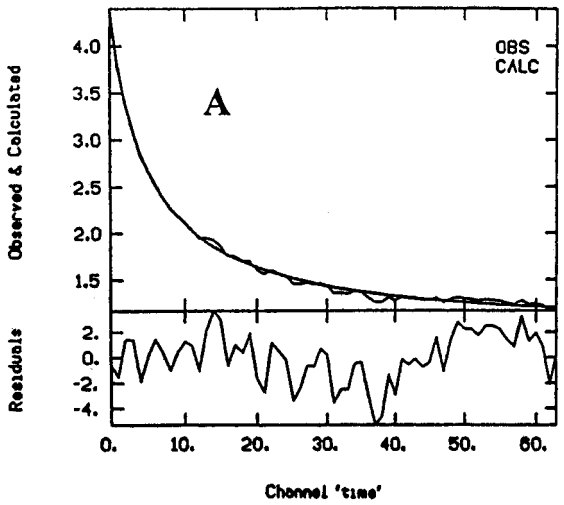

Figure 29. First published single molecule FCS autocorrelation function at ambient temperature and theoretical fit. The difference between theory and experiment is shown in the bottom panel. The average occupancy in the probe volume was determined from the fit to be 0.005, and the diffusion time through the probe volume was 43 μs. Reprinted with permission from: Rigler, R.; Mets, Ü. *Proc. SPIE* **1992**, *1921*, 239−248. Copyright 1992 International Society for Optical Engineering.

Several interesting FCS studies were performed on DNA molecules under conditions adequate for single molecule detection.[67,84,137−144] FCS was used to monitor the kinetics[136−138] and extract the activation energies[137] for the hybridization of fluorescently tagged DNA's to their complements. The exonuclease digestion of fluorescently labeled DNA was observed,[67,139,140] which has allowed rapid screening of exonucleases that may be of use in single molecule DNA sequencing (section II.H.1). The replication of DNA in polymerase chain reactions (PCR) has been monitored by FCS.[142,144] Another interesting application, being investigated by Kinjo and co-workers, involves using FCS to detect single point mutations

in genes by analyzing the exact number of fragments produced by a restriction digest.[141,143]

Several protein and enzyme molecules were investigated by FCS at the single molecule level. The dynamics of fluorescence fluctuations of individual molecules of Green Fluorescent Protein (GFP) were studied, yielding kinetic information that would be masked in bulk fluorescence measurements.[145] Another study used FCS to monitor the interaction between carbohydrates and proteins.[146] The conformational change of H^+-ATPase that takes place upon binding to nucleotides was monitored by FCS.[147] Single molecule FCS was also used to study the binding of individual histidine-tagged molecules to chelator lipids.[148]

Another study used FCS to measure singlet−triplet crossing rates in fluorophores.[149,150] Two detectors were used to improve the timing resolution necessary to see these short time scale fluctuations. A study of the quenching dynamics of dye molecules with various nucleotides employed a similar setup.[151]

Two detectors can also be used to detect simultaneously two fluorophores of different colors. By performing a cross-correlation between the two detectors, one can quickly identify molecules that contain both fluorophores as they diffuse through the laser probe volume.[90,152] To minimize cross-talk, two different band-pass filters and spectrally well-separated dyes are generally used for this analysis. This dual color cross-correlation technique was used to identify target DNA sequences in PCR.[153] DNA−DNA renaturization kinetics have been followed,[152] and endonuclease digestion has been monitored.[154] Dual color cross-correlation techniques have a fairly simple mathematical evaluation and shorter readout times than conventional FCS.[154] This technique thus holds promise of reducing the analysis time needed for high throughput screening.[155]

V. Single Molecule Spectroscopy in Microcapillaries and Microstructures

The importance of the use of small detection volumes to reduce contributions from background was discussed in the Introduction. This section describes the use of capillaries and microchannels to confine samples to small probe volumes.

The use of capillaries to confine the sample stream to a small probe volume suitable for single molecule detection was reported by Winefordner and co-workers.[13] An ultradilute solution of the fluorescent dye IR140 dissolved in methanol was passed through an 11 μm i.d. capillary. The excitation laser (780 nm) was focused to a $1/e^2$ diameter of 11 μm to irradiate the entire cross section of the capillary. All of the analyte molecules passed through the 1 pL detection volume. Scattered excitation light from the capillary walls was reduced with a rubidium metal vapor filter (absorbance ~8 at 780 nm). Bursts of photons associated with the passage of single molecules through the probe volume were observed with good signal-to-noise ratios. Because of the Gaussian spatial distribution of the excitation laser, the Poiseuille flow velocity profile, and photobleaching of analyte molecules, a large variation in the burst sizes from individual molecules was observed. A detection efficiency >90% was reported.

Further work by the same authors demonstrated the use of two sequential probe volumes to discriminate against false positive signals associated with Rayleigh and Raman scattering.[156] Two parallel laser beams, separated by 2.8 mm, irradiated the capillary tube containing the sample. The transit time between the two probe volumes was 230 ms. Photon bursts attributed to single molecules were detected in the two channels with a time difference corresponding to the transit time of a molecule between the probe volumes. Cross-correlation of the signal from the two detection channels yielded a peak corresponding to the transit time between the two probe volumes.

As described in section IV, confocal excitation and detection results in excellent signal-to-noise ratios but low detection efficiencies. The low detection efficiencies result from sample volumes large with respect to the probe volume; most of the analyte molecules do not pass through the probe volume. In addition, diffusion of molecules in and out of the probe volume complicates the interpretation of the data.

Confocal microscopy was used to detect single molecules inside of micromachined channels on silicon.[157] Bursts were detected with good signal-to-noise but the background from the microchannel was large. Again, the dimensions of the detection volume were much smaller than the microchannel dimensions and the detection efficiency was small.

An interesting solution to this problem was reported by Dörre et al.[67] The entire cross section of a microchannel was illuminated with laser light and fluorescence was imaged onto an array of seven adjacent, 50 μm diameter, multimode optical fibers acting as pinholes in a confocal detection scheme. The output of each fiber was imaged onto a different avalanche photodiode. The result was a line of overlapping femtoliter probe volumes spanning the microchannel. Every molecule passed through one of the probe volumes. Single molecule detection was reported with a signal-to-noise ratio of ~4. This arrangement was used with two color excitation and two color detection (14 fibers and 14 detectors) to distinguish between tetramethylrhodamine and Cy5 flowing through the microchannel.

Capillary tubes and microstructures with internal dimensions < 1 μm have been used to confine the sample stream to the center of femtoliter probe volumes in an attempt to improve the detection efficiency of confocal spectroscopy. A pulled capillary with an internal diameter of 500−600 nm was used to constrain single R6G molecules to flow through a 1−2 fL probe volume.[158] The molecular residence time in the absence of flow was approximately 60 ms. During this time, a burst of several thousand photons was recorded from a single molecule. In contrast, the diffusion time across a femtoliter probe volume in bulk solution is ~1 ms. The increased diffusion time in the nanobore capillary was attributed to an attractive interaction of the positively charged R6G with the negative charge on the capillary wall. Electroosmotic flow was used to move analyte molecules through the probe volume.

Zander et al. used a similar system to count single R6G molecules passing through a femtoliter probe volume in a 1 μm i.d. capillary tube.[159] A flow velocity of 500 μm/s was induced by capillary action. The observed count of 21 molecules in 10 s is in excellent agreement with a calculated count of 24 molecules. This is quantitative analysis at the single molecule level. Subsequently, Zander et al. demonstrated the use of confocal excitation and time-correlated detection with pulsed diode laser excitation for single molecule counting and identification of dye-labeled nucleotides passing through a 500 nm diameter tip on the end of a capillary (commercially available "Femtotip").[160] Electroosmotic forces were used to pass a mixture of Cy5-dCTP and JA53-dUTP (a rhodamine derivative) through the capillary. The excitation laser was focused just inside the exit of the capillary. Molecules were detected, counted, and identified by their fluorescence lifetime as described in section II.G.2.b. The detection efficiency was limited because only large bursts were analyzed.

Single molecule detection was used to measure the partition coefficients and photophysical properties of single NIR fluorescent dye molecules within micelles.[44] A focus of the research was to determine the homogeneity of the intramicelle environment. The results indicated that the dye molecules inside the micelles experience similar microenvironments—inhomogeneities were not observed.

VI. Single Molecule Spectroscopy by Two-Photon Excitation

Recently, it was demonstrated that single molecule detection can be accomplished using two-photon fluorescence excitation.[20,161−166] Most of the two-photon single molecule studies that have been reported to date have utilized two-photon fluorescence microscopy. The principles of two-photon microscopy were first elucidated by Webb and co-workers[167] and are the subject of several recent review articles. See for example So et al.[168]

Two-photon microscopy differs from standard confocal fluorescence microscopy techniques that are based on one-photon excitation (OPE) in several respects. In two-photon microscopy, the analyte molecules are excited to their fluorescent state by the simultaneous absorption of two photons with a total energy corresponding to the excitation energy of the molecule. For example, for a visible or near-UV chromophore, two-photon excitation (TPE) is achieved by the absorption of two near-infrared photons. The cross sections for TPE are extremely small, typically on the order of 10^{-50} cm^4 s/photon for most fluorophores.[169] Thus, the high instantaneous irradiance provided by a tightly focused, short pulse width ($\sim$100 fs) laser, such as a mode-locked Ti:sapphire laser, is required to achieve appreciable TPE rates. TPE is a nonlinear process, wherein the molecular excitation rate depends quadratically on the intensity of the excitation laser. In two-photon microscopy, the excitation laser is focused to a near-diffraction limited spot of less than 1 μm in diameter. The three-dimensional spatial resolution of this technique arises from the large spatial variation in the two-photon excitation rate across the focal region of the laser beam, such that appreciable two-photon excitation occurs only at the laser beam focus.

Several advantages to using two-photon microscopy, as opposed to conventional confocal microscopy, have been realized. For example, since excitation occurs only at the laser beam focus, the remainder of the sample is not subject to photodamage. Also, the effective probe volume for two-photon microscopy is somewhat smaller than for confocal microscopy because of the quadratic dependence on the intensity, resulting in improved spatial resolution. Finally, because of the large spectral separation between the excitation and detection wavelengths, background radiation due to Rayleigh and Raman scattering of the excitation laser beam by the sample can be completely suppressed with optical filters, while still collecting the entire fluorescence emission spectrum with high efficiency. Thus, it is often possible to achieve a higher fluorescence detection sensitivity using TPE as compared to OPE.[170,171]

In 1995, Webb and co-workers demonstrated that two-photon fluorescence microscopy could be applied to the detection of single molecules in solution.[20] These authors used a mode-locked, 100 fs pulse width (broadened to $\sim$250 fs by group delay dispersion), 795 nm Ti:sapphire laser, focused to a beam waist of 750 nm, to excite single Rhodamine B (RhB) molecules in a 6 pM aqueous solution as they diffused through the $\sim$1 fL detection volume. The repetition rate of the laser was doubled to 152 MHz using an optical delay line. The average laser power was 36 mW, corresponding to a peak irradiance of $\sim 10^{30}$ photons/(cm^2 s). Under these conditions, photon bursts from single RhB molecules of $\sim$0.7 ms in duration could be detected with an average number of detected photons per burst of $\sim$1. Although the burst sizes for single molecules were much less than those observed using one-photon confocal detection, the background count rate was reduced by more than 1 order of magnitude using TPE. The authors reported an overall signal-to-background ratio that was slightly better than that observed by OPE.

More recently, Brand and co-workers used two-photon fluorescence microscopy with 700 nm excitation to study single molecules of the UV chromophore Coumarin-120 (C-120) in aqueous solution.[162,172,173] The two-photon fluorescence microscopy technique was similar to that used by Webb and co-workers to study RhB, except that time-resolved measurements were used to identify the individual C-120 molecules on the basis of their characteristic fluorescence lifetimes. These authors studied the various sources of background radiation as a function of the excitation laser power and found that white light continuum generation occurs above a peak irradiance of $\sim 10^{31}$ photons/(cm^2 s). This value for the peak photon flux was beyond the saturation intensity for two-photon excitation of C-120. Other sources of background encountered in TPE experiments include hyper-Rayleigh and hyper-Raman scattering[174] and TPE of fluorescent impurities. Brand et al. also studied fluorescence bursts from single C-120 molecules using OPE at 350 nm.[162] Figure 30 compares the results for OPE (Figure 30a) and TPE (Figure

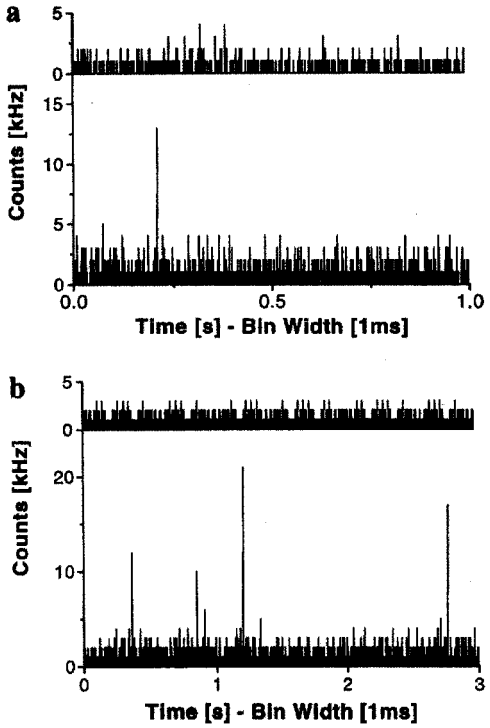

Figure 30. Time-resolved fluorescence signal from a 10^{-11} M solution of Coumarin-120 in water using (a) OPE at 350 nm (average irradiance 7×10^{22} photons/(cm^2 s)) and (b) TPE at 700 nm (average irradiance 2×10^{26} photons/(cm^2 s)). The upper traces in (a) and (b) are from a pure water blank. Reprinted from: Brand, L.; Eggeling, C.; Zander, C.; Drexhage, K. H.; Seidel, C. A. M. *J. Phys. Chem. A* **1997**, *101*, 4313−4321. Copyright 1997 American Chemical Society.

30b). An important conclusion of these studies was that the single molecule detection sensitivity for C-120 was enhanced by a factor of ~3 using TPE as compared to OPE. This was due to the high background that occurs due to OPE at UV wavelengths and the superior background suppression capability of TPE.

The advantages of two-photon microscopy have also been realized in fluorescence correlation spectroscopy.[175,176] In particular, Berland et al. applied these techniques to characterize the intracellular environment.[175] These authors measured the diffusion coefficients of fluorescent beads, 7 and 15 nm in diameter, injected into the cytoplasm of mouse fibroblast cells. Two-photon microscopy enabled them to perform these measurements without subjecting the sample to photodamage.

Several groups have reported two-photon microscopy studies of single molecules on room-temperature glass surfaces[163−165] and doped in solid samples at cryogenic temperatures.[161,177,178] The room-temperature measurements were accomplished using both far-field[163,164] and near-field microscopy.[165] Sánchez et al. used a 180 fs pulse width, 840 nm Ti:sapphire laser to excite single RhB molecules in the far-field.[163] The RhB molecules were affixed to a glass surface, and the surface was scanned with respect to the laser beam to obtain single molecule fluorescence images (see Figure 31). The spatial resolution that was obtained for these images was ~250 nm, which is smaller than the value typically achieved using OPE,

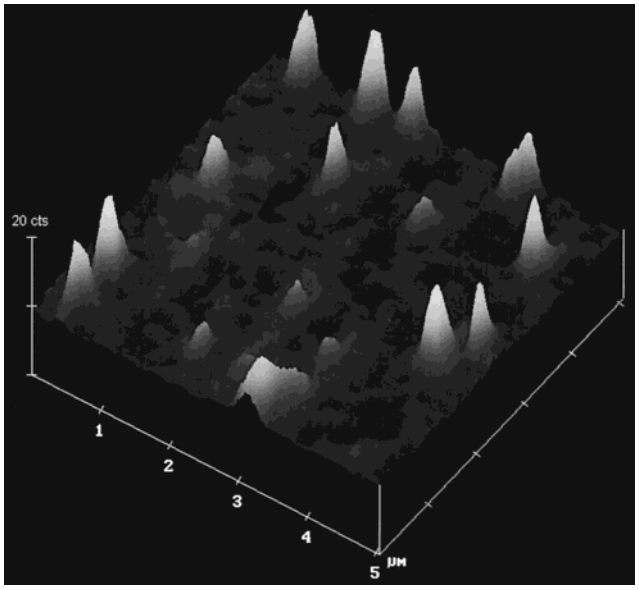

Figure 31. Fluorescence image of single RhB molecules on a glass surface obtained by two-photon excitation. The spatial resolution was 250 nm. Reprinted from: Sánchez, E. J.; Novotny, L.; Holtom, G. R.; Xie, X. S. *J. Phys. Chem. A* **1997**, *101*, 7019−7023. Copyright 1997 American Chemical Society.

due to the quadratic intensity dependence of the TPE rate. These authors also compared the average time to photobleaching for single molecules excited by one and two photons and found that the photobleaching probability for TPE was about two times larger than for OPE. They speculated that multiphoton processes could be responsible for the higher photobleaching rates observed for TPE.

There are many potential advantages to using TPE in conjunction with near-field scanning optical microscopy (NSOM), including the low background and the low fluorescence excitation of the sample outside the near-field region of the probe tip. Until very recently, however, the excitation intensity from the small aperture of the near field tip was not sufficient to induce a detectable level of single molecule fluorescence with TPE. Lewis et al.[165] overcame this problem by using an uncoated NSOM tip to increase the excitation intensity. These authors used an 800 nm, 100 fs pulse width Ti:sapphire laser beam, transmitted through an optical fiber with a 200 nm diameter tip, for near-field excitation of single RhB molecules on a glass surface. Single molecule fluorescence images were obtained with a spatial resolution of 175 nm. They also observed the same increase in the photobleaching probability compared to OPE reported by Sánchez et al.[163]

The utility of TPE in applications that involve single molecule detection is hindered somewhat by the low two-photon absorption cross sections for most fluorescent molecules. Although the level of background interference due to TPE is certainly much lower than for OPE, it is usually not possible to achieve single molecule excitation rates that are comparable to OPE. Therefore, in most cases, the overall single molecule detection sensitivity is not significantly enhanced by TPE. These challenges may soon be overcome due to the recent development of a

new class of fluorescent bis(styryl)benzene derivatives that possess extraordinarily large two-photon absorption cross sections.[179,180] For example, several of the bis(styryl)benzene derivatives described by Albota et al. possess two-photon absorption cross sections above 10^{-47} cm^4 s/photon and high fluorescence quantum yields (between 0.8 and 0.9).[180] By comparison, RhB possesses a maximum two-photon absorption cross section of 1.5×10^{-48} cm^4 s/photon.[169] This new class of fluorophores may open the possibility for many new applications for single molecule detection by TPE.

VII. Single Molecule Imaging under Ambient Conditions with Cameras

VII.A. Overview

In this section, we discuss single fluorophore imaging with two-dimensional array detectors. From a historical perspective, it has been possible to detect the positions of single macromolecules decorated with ~100 fluorophores for more than 20 years.[1] More recently, sensitive cameras have been used to image the fluorescence from single fluorophores at liquid-helium temperatures.[181] Cameras have been used in combination with spectrometers for emission and lifetime spectroscopy by dispersing wavelengths or fluorescence-decay times.[15,24,35,182−191] We confine our discussion to recent imaging applications of single fluorophores under ambient conditions.[12,19,21−23,27,191−220]

One may ask why it is interesting to observe the emission from a single fluorophore with a camera, since several hundred fluorophore labels can be attached within a diffraction limited spot. In contrast to observing the position of a single macromolecule with many fluorophore labels, a single fluorophore provides additional information: polarization or image spot shapes indicate orientation and reorientation;[7,164,203,208,217,221,222] time traces of the intensity, emission spectrum, or fluorescence lifetime provide information on local dynamics;[11,15,19,22,24,35,36,39,162,164,194,197,198,200,205,206,215,223] energy transfer provides information on the proximity of specific labeled sites less than 10 nm apart.[24,42,213,224] Position sensitivity allows an investigator to locate a molecule and to follow simultaneously the translational motion, reorientational motion, and the internal dynamics of individual molecules.

The types of samples amenable to study by cameras depend on the temporal and spatial resolution. The temporal resolution and position precision can be as high as ~10 ms and ~30 nm. Consider a single fluorophore as either rapidly diffusing in solution or being constrained in motion. As shown in previous sections of this review, fully solvated molecules tend to be studied with single element detectors by virtue of their high timing resolution. Single element detectors have been used also to study constrained molecules with scanning techniques such as scanning near-field[7,11,15,16,24,36,222,224−227] or scanning confocal microscopies.[185,186,221,224,228] Single molecule detection using scanning microscopies has been described in many reviews.[35−42] Sensitive, two-dimensional cameras do not have timing resolution as high as single element detectors, but they do have other distinguishing attributes: many signals are detected simultaneously, and the constrained motion of individual fluorophores can be followed.

One of the compelling aspects of single molecule studies is the ability to observe directly distributions of individual properties and molecular behavior. Obtaining distributions of such parameters requires studying a large number of individual molecules. The high parallelism inherent in a camera yields the properties of a large number of individual molecules simultaneously. Examples of the types of motion and dynamics observed with single fluorophore labels are discussed below.

VII.B. Technical Challenges and Solutions

A camera with low light level sensitivity can be used to observe the motion of single fluorophores with limitations on the temporal and positional resolution. In the visible spectral region, the image spot size and spatial resolution are limited by diffraction to about ~300 nm. Two molecules with similar emission spectra can be resolved if they are further apart than ~300 nm. The spatial precision in the position of a single molecule is higher than the ability to resolve two molecules. The position precision depends on the spot size, the number of available photoelectrons, and the shot noise in the measurement. In the presence of photobleaching, the mean number of detected photons from a single molecule is on the order of 10^3−10^4. Within the limitation of the total available light, the position can be determined to within tens of nanometers. The speed of present-day cameras does not match the ~100 ps temporal resolution of single element detectors such as PMTs or SAPDs. Color film requires at least seconds of exposure at the light levels available from single molecules and additional development time. Electronic cameras are faster than film and require milliseconds to seconds of readout time. Hence, for direct observation of the behavior of single molecules, the temporal resolution has been limited to processes with kHz or slower rates. The motion of a fluorophore can be measured with tens of nanometer precision and with a temporal resolution of milliseconds.

Signal-to-noise ratio considerations determine the total number of resolvable molecules in an image and the kinds of motion that can be observed. Because the number of photoelectrons is limited by photobleaching, a large fraction of the emitted light must be detected. A large collection half-angle, θ, can be obtained by using a large numerical aperture microscope objective (NA = $n \sin \theta$; n is the index of refraction at the sample position). Commercial objectives with high NA (1.0−1.65) tend to have a working field-of-view of several hundred micrometers or less. With a low enough coverage to prevent overlap of the ~300 nm spots, it is possible to resolve several hundred molecules individually and simultaneously. A large NA produces a depth of focus less than several micrometers. Hence, the kinds of motion that can be observed are constrained laterally to several hundred micrometers and in depth to less than a few micrometers. For this reason, samples that have been studied have somewhat restricted motion and tend to be on or near interfaces.

Single molecules are detected only when they are in focus, but background can originate from both in-focus and out-of-focus volumes. Single element detectors are usually used in combination with a spatial filter (small aperture in an image plane) to reduce optical background from out-of-focus volumes. For wide-field imaging, the size of the spatial filter must be increased.

Various methods other than spatial-filtering and time-gating have been explored for reducing the background contribution from out-of-focus volumes. A conventional mode of fluorescence excitation in wide-field microscopy is epi-illumination.[21,22,191,193,194,196,199,201−203,207,208,213,218] In epi-illumination, the excitation and emission light travel through the same optics. To reduce the background scatter, optics must be of high quality and produce very little longer-wavelength luminescence. Another method of background reduction is to limit the field of view to about 30 diffraction limited diameters (about 10 μm)—a compromise between wide-field and confocal. Under these conditions, signal-to-background ratios (SBR) of 7−10 and signal-to-background-noise ratios (SBNR) of 70−170 have been achieved with 35−40 ms of illumination above ~10 kW/cm^2.[22,213]

Another method of background reduction is to remove the excitation light from the emission-collection optics. One of the first wide-field imaging studies used external reflection from the sample surface by inserting the laser beam between the sample and the microscope objective.[12,212] Another effective alternative to epi-illumination is total internal reflection (TIR) excitation at a glass surface.[19,23,27,195,197,198,200,205,206,210,211,215−217,220] See Figure 32 for diagrams of various TIR geometries. The

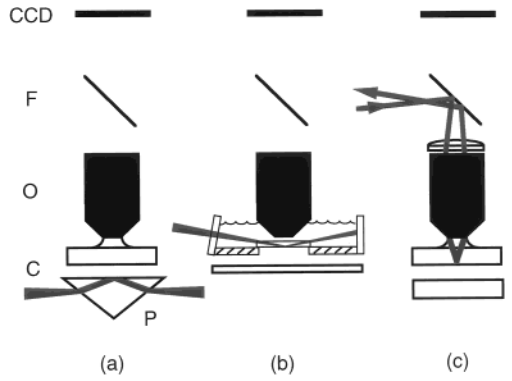

Figure 32. Various total internal reflection (TIR) excitation geometries. Labels in the figure are the following: CCD, charge coupled device camera; F, dichroic beam splitter used as a long pass filter; O, high numerical aperture microscope objective; C, sample cell formed from a gap between two silica surfaces; P, silica prism. In these examples, the objective, O, is designed to work with immersion oil and a cover glass. Total internal reflection can be performed on either silica surface of the sample cell, C. (a) Prism TIR is performed on the bottom of the sample cell by reflecting a laser beam from a silica surface within a prism, P. (b) Prismless TIR can be obtained by inserting a narrow beam between the objective and the top cover slip. (c) Prismless through objective TIR occurs for large-angle input rays that focus beyond the critical angle at the top silica surface. Reprinted with permission from: Ambrose, W. P.; Goodwin, P. M.; Nolan, J. P. *Cytometry* **1999**, *36*, 224−231. Copyright 1999 Wiley.

reflection from a high-to-low refractive index step is total for incident angles larger than a critical angle measured from the surface normal.[229,230] Since the reflection is total, an evanescent optical field travels along the surface with an exponentially decaying field amplitude into the lower index medium. The extent of the evanescent field varies with incident angle and can be as small as ~100 nm. Except for small amounts of scattered light, TIR excitation light does not illuminate the collection optics. In comparison to epi-illumination, TIR-illumination in a field-of-view of tens of micrometers diameter increases the SBR from about 3 to 12.[19,205,220] See Figure 33 for examples

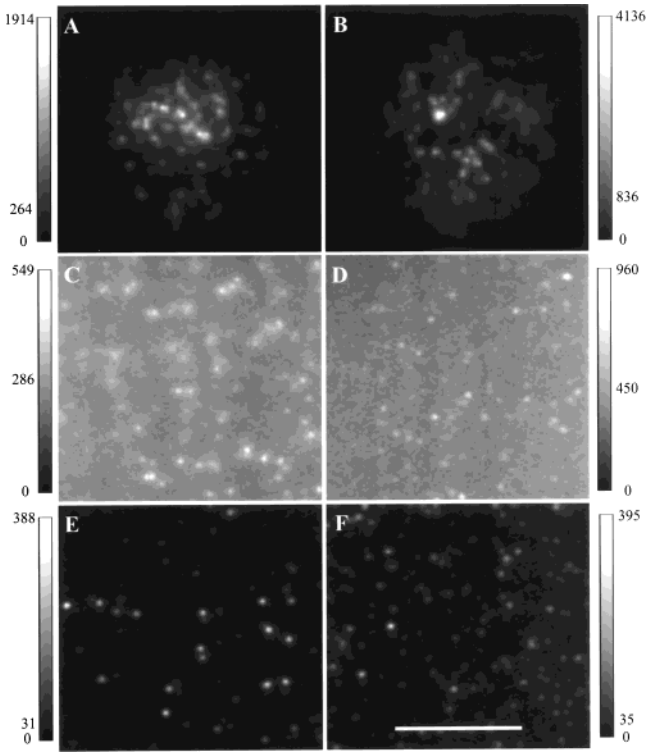

Figure 33. Images of the fluorescence detected from single molecules showing different signal-to-background ratios obtained with various TIR excitation geometries. See Figure 32 for the corresponding geometries. (A) and (B) are images obtained with through-objective TIR excitation. (C) and (D) are images obtained with between-the-objective-and-cover-slip TIR excitation. (E) and (F) are images obtained with prism TIR. The images on the left (A, C, E) show the locations of individual Rhodamine 6G molecules at air−silica interfaces. The images on the right (B, D, F) are of individual B phycoerythrin proteins at the interface between a buffer solution and silica. The white, 10 micrometer scale bar in (F) is the same for all images. The gray scales are adjusted to normalize the largest signal in each image to white. The nonzero labels on each gray scale bar are the largest signals-plus-background and the background level. Reprinted with permission from: Ambrose, W. P.; Goodwin, P. M.; Nolan, J. P. *Cytometry* **1999**, *36*, 224−231. Copyright 1999 Wiley.

of the SBR that can be obtained with various TIR geometries.

VII.C. Sensitive Cameras

Various types of cameras have been used for wide-field imaging of single fluorophores under ambient conditions. Color photographic film has been used to

record surface enhanced resonance Raman scattering (SERS) from single molecules.[187] A small fraction of individual silver colloid particles with a single fluorophore adsorbed exhibit an extremely large Raman scattering signal, comparable in size to the fluorescence emission rate (a detailed description of SERS is the subject of another article of this special issue). High photostability of these rare, bright molecule−particle combinations allows them to scatter numbers of photons well in excess of the mean number expected from fluorescence. Hence, an old imaging workhorse, color photographic film, has been used to image the locations of the brightest particles immobilized on a glass slide. Photographic film is slower than an electronic camera, but it does provide spectral sensitivity (color).

Most other wide-field single molecule experiments have used fluorescence excitation and detection with electronic cameras. Cooled, silicon charge-coupled device (CCD) arrays are available with low readout noise (several electrons root-mean-square, RMS), low dark charging rate (<0.1 electrons per pixel per hour), and a well depth of $\sim 10^5$ photoelectrons. Since the RMS readout noise is more than one electron, several tens of photons must be detected per pixel. In other words, cooled CCDs are low light level detectors but are not single photon counting devices. To achieve low readout noise, the readout bandwidth must be limited to 50 kHz; i.e., the image readout time can be many seconds. Charge shifting before readout can be performed with high efficiency and very little addition of noise. Rapid imaging for a limited number of frames has been performed with a cooled CCD by restricting the image area and shifting the image charge into dark pixels.[22,27,194,202,203,216] A short run of images with millisecond integration times can be obtained by charge shifting before readout until the CCD array is filled.

CCD arrays can be read out continuously at NTSC-video frame rates (33 ms/frame), but the readout bandwidth and noise are much higher than with slow-scan CCD cameras. To overcome the high readout noise, an image intensifier can be used as a photon amplifier in combination with a CCD (known as an ICCD).[197,217,220] Intensifiers are available with front-end photocathodes having quantum efficiencies comparable to silicon (~40%). A single amplified photon can produce a mean number of electrons on the CCD that is higher than the readout noise; i.e., single photon counting can be accomplished with an ICCD. A trade off for single photon counting sensitivity in an ICCD is that the full well depth of the camera is reduced from $\sim 10^5$ to $\sim 10^2$ detected photons. Another type of camera with single photon counting sensitivity at video rates is an intensified silicon target (ISIT) camera. Essentially, the multichannel plate/phosphor conversion step in an intensifier is replaced with photoelectrons directly accelerated to a silicon detector.[12,19,21,191,195,196,198−200,205−208,210−212,214,215]

VII.D. Translational Motion

Constrained diffusional motion of single fluorophores has been studied using the position imaging capabilities of sensitive cameras. The two-dimensional motion of labeled lipids was observed in both supported and free-standing lipid layers and on cell surfaces.[22,194,201] Differences in the diffusion of individual molecules were observed, consistent with different domains of fluidity being influenced by the supporting medium. An advantage of this technique over bulk diffusion measurements is that bulk measurements are diffraction limited (~300 nm resolution) whereas single molecule centroid determinations are much better than diffraction limited (~30 nm). Constrained, three-dimensional diffusion of molecules near an interface has been studied.[23] Molecules were placed in a hydrated porous gel between cover slips. Fluorophores near the gel−silica interface were excited using TIR illumination. In addition to observing the lateral motion of the molecules, the distance from the surface could be discerned by correlating the emission intensity to the excitation rate in the evanescent field. Restricted diffusion in an aqueous solution also has been examined.[27,216] Diffusion in liquids is very rapid in comparison to the spatio−temporal resolution of present-day cameras. A small fluorophore will diffuse several micrometers in a millisecond. For these studies, the molecules were constrained within the depth of field by using a cover slip separation of 4 μm. The image spots were larger than diffraction limited, indicative of the diffusive motion of the molecule within the image acquisition time.[27] In related work, the diffusive motion of molecules in a buffer solution adjacent to a charged silica surface exhibited a surprising effect.[216] The static electric field near a charged surface is screened by buffer ions. Calculations show the range that the field should influence diffusion of charged molecules should be only 3 nm. Instead, the diffusive motion of charged molecules was influenced over a distance of 180 nm into the buffer. The observation of single molecule diffusion should improve our understanding of important separation technologies such as capillary electrophoresis.

Individual molecular motor components have been extracted from cells and studied in vitro. The motion of singly labeled molecular motors traveling on protein filaments has been observed for myosin on actin filaments[206,215] and kinesin on microtubules.[192,198] One-dimensional diffusion of RNA polymerases nonspecifically bound to DNA has been observed recently.[219] Such experiments shed light on the mechanisms involved in molecular motors and will be useful for elucidating the details of DNA−RNA transcription.

VII.E. Reorientational Motion

Single fluorophores have polarized transition dipole moments. The orientation of the in-plane component of the dipole can be determined by measuring polarized absorption and emission. The out-of-plane component can be discerned by differences in the diffraction ring pattern generated by aberrations in the optical system.[217] Reorientation is observed as changes in pairs of orthogonally polarized images. In free solution, reorientation occurs on time scales much

shorter than milliseconds—typically picoseconds for small molecules. By the attachment of fluorophores rigidly to macromolecules, the slower reorientational motion of the macromolecule is observed. The fluidity of a lipid membrane has been observed at specific sites by observing the polarization changes in labeled lipids.[203]

Reorientation has been observed simultaneously with molecular motor motion. Labels attached to actin filaments were observed to rotate by comparing two orthogonally polarized images.[208] As a filament translated relative to immobilized myosin motors the emission polarizations alternated. Surprisingly, the period of rotation does not correspond to the spiral groove in the filament, which supports speculation about myosin-motor hopping motions rather than walking.

F1-ATPase is a component of a larger structure responsible for conversion of a membrane proton gradient into chemical energy stored in ATP. Rotation of the central-axis protein in F1-ATPase was observed directly.[199,207,214] Individual steps of 120° were observed during ATP hydrolysis at low ATP concentration. Hydrodynamic drag on a lever arm (actin filament attached to the central rotor) allows measurement of the torque and work per motor step. Within experimental error, the measurements are consistent with 100% conversion of chemical energy to rotational work. Heterogeneity in the rotation behaviors of F1-ATPase attached to a solid substrate was observed. More work is needed to distinguish environmental heterogeneity from molecular heterogeneity.

VII.F. Intensity Fluctuations and Chemical Kinetics

The emission rate from a single fluorophore can be sensitive to its environment and to its previous excitation history. Intensity fluctuations are ubiquitous in studies of constrained single molecules. The interpretations for the sources of the fluctuations appear to be as varied as the different samples studied. Examples are light-induced blinking behavior of Green Fluorescent Proteins associated with the charge state of the chromophore,[197] and conformational changes influencing fluorophore labels.[39,42]

Cameras have been used to monitor the accumulation of products catalyzed by many individual enzymes or metal ions in parallel.[204] Individual association−dissociation events occurring during chemical reactions have been observed through intensity fluctuations. To observe individual and repeated chemical events with high timing resolution, single element detectors are used in confocal microscopy.[42,231]

A position-sensitive camera provides complementary information on molecular motor motion induced by chemical reactions.[21,192,198,199,207,208,214,215] Many molecular motors derive energy for motion from ATP−ADP reactions. Association−dissociation kinetics of ATP with myosin have been observed by labeling ATP with one color and myosin with another.[19,198,200,205] The myosin was immobilized on a cover slip, and binding times of individual ATPs were monitored. Combining such observations with force measurements has produced controversial speculation about the storage of energy in the motor and the size of the step.[211,232] Association−dissociation kinetics of RNA transcriptase proteins with DNA have been observed to vary with the tension applied to the DNA and with the location on the DNA (depending on whether the site is a nonspecific binding site or if the local DNA sequence closely resembles known binding sites).[219]

VIII. Reference

(1) Hirschfeld, T. *Appl. Opt.* **1976**, *15*, 2965−2966.
(2) Dovichi, N. J.; Martin, J. C.; Jett, J. H.; Keller, R. A. *Science* **1983**, *219*, 845−847.
(3) Dovichi, N. J.; Martin, J. C.; Jett, J. H.; Trkula, M.; Keller, R. A. *Anal. Chem.* **1984**, *56*, 348−354.
(4) Shera, E. B.; Seitzinger, N. K.; Davis, L. M.; Keller, R. A.; Soper, S. A. *Chem. Phys. Lett.* **1990**, *174*, 553−557.
(5) Soper, S. A.; Shera, E. B.; Martin, J. C.; Jett, J. H.; Hahn, J. H.; Nutter, H. L.; Keller, R. A. *Anal. Chem.* **1991**, *63*, 432−437.
(6) Barnes, M. D.; Ng, K. C.; Whitten, W. B.; Ramsey, J. M. *Anal. Chem.* **1993**, *65*, 2360−2365.
(7) Betzig, E.; Chichester, R. J. *Science* **1993**, *262*, 1422−1425.
(8) Li, L.-Q.; Davis., L. M. *Rev. Sci. Instrum.* **1993**, *64*, 1524−1529.
(9) Rigler, R.; Widengren, J.; Mets, Ü. In *Fluorescence Spectroscopy*; Wolfbeis, O. S., Ed.; Springer-Verlag: Berlin, 1993.
(10) Soper, S. A.; Mattingly, Q. L.; Vegunta, P. *Anal. Chem.* **1993**, *65*, 740−747.
(11) Ambrose, W. P.; Goodwin, P. M.; Martin, J. C.; Keller, R. A. *Phys. Rev. Lett.* **1994**, *72*, 160−163.
(12) Ishikawa, M.; Hirano, K.; Hayakawa, T.; Hosoi, S.; Brenner, S. *Jpn. J. Appl. Phys., Part 1* **1994**, *33*, 1571−1576.
(13) Lee, Y. H.; Maus, R. G.; Smith, B. W.; Winefordner, J. D. *Anal. Chem.* **1994**, *66*, 4142−4149.
(14) Nie, S.; Chiu, D. T.; Zare, R. N. *Science* **1994**, *266*, 1018−1021.
(15) Trautman, J. K.; Macklin, J. J.; Brus, L. E.; Betzig, E. *Nature* **1994**, *369*, 40−42.
(16) Xie, X. S.; Dunn, R. C. *Science* **1994**, *265*, 361−364.
(17) Li, L.-Q.; Davis, L. M. *Appl. Opt.* **1995**, *34*, 3208−3217.
(18) Castro, A.; Shera, E. B. *Anal. Chem.* **1995**, *67*, 3181−3186.
(19) Funatsu, T.; Harada, Y.; Tokunaga, M.; Saito, K.; Yanagida, T. *Nature* **1995**, *374*, 555−559.
(20) Mertz, J.; Xu, C.; Webb, W. W. *Opt. Lett.* **1995**, *20*, 2532−2534.
(21) Sase, I.; Miyata, S. I.; Jet, C.; Craik, J. S.; Kinosita, K. *Biophys. J.* **1995**, *69*, 323−328.
(22) Schmidt, T.; Schütz, G. L.; Baumgartner, W.; Gruber, H. J.; Schindler, H. *J. Phys. Chem.* **1995**, *99*, 17662−17668.
(23) Dickson, R. M.; Norris, D. J.; Tzeng, Y.-L.; Moerner, W. E. *Science* **1996**, *274*, 966−969.
(24) Ha, T.; Enderle, T.; Ogletree, D. F.; Chemla, D. S.; Selvin, P. R.; Weiss, S. *Proc. Natl. Acad. Sci. U.S.A.* **1996**, *93*, 6264−6268.
(25) Sauer, M.; Drexhage, K. H.; Zander, C.; Wolfrum, J. *Chem. Phys. Lett.* **1996**, *254*, 223−228.
(26) Zander, C.; Sauer, M.; Drexhage, K. H.; Ko, D.-S.; Schultz, J.; Wolfrum, J.; Brand, L.; Eggeling, C.; Seidel, C. A. M. *Appl. Phys. B* **1996**, *63*, 517−523.
(27) Xu, X.-H.; Yeung, E. S. *Science* **1997**, *275*, 1106−1109.
(28) Bopp, M. A.; Jia, Y. W.; Li, L. Q.; Cogdell, R. J.; Hochstrasser, R. M. *Proc. Natl. Acad. Sci. U.S.A.* **1997**, *94*, 10630−10635.
(29) Vanden Bout, D. A.; Yip, W. T.; Hu, D. H.; Fu, D. K.; Swager, T. M.; Barbara, P. F. *Science* **1997**, *277*, 1074−1077.
(30) Yip, W. T.; Hu, D.; Yu, J.; Vanden Bout, D. A.; Barbara, P. F. *J. Phys. Chem. A* **1998**, *102*, 7564−7575.
(31) Barnes, M. D.; Whitten, W. B.; Ramsey, J. M. *Anal. Chem.* **1995**, *67*, 7, A418−A423.
(32) Castro, A.; Shera, E. B. *Appl. Opt.* **1995**, *34*, 3218−3222.
(33) Keller, R. A.; Ambrose, W. P.; Goodwin, P. M.; Jett, J. H.; Martin, J. C.; Wu, M. *Appl. Spectrosc.* **1996**, *50*, 12A−32A.
(34) Goodwin, P. M.; Ambrose, W. P.; Keller, R. A. *Acc. Chem. Res.* **1996**, *29*, 607−613.
(35) Xie, X. S. *Acc. Chem. Res.* **1996**, *29*, 598−606.
(36) Trautman, J. K.; Ambrose, W. P. In *Single-Molecule Optical Detection, Imaging and Spectroscopy*; Basché, T., Moerner, W. E., Orrit, M., Wild, U. P., Eds.; VCH Verlagsgesellschaft, mbH: Weinheim, Germany, 1997; pp 191−222.
(37) Nie, S.; Zare, R. N. *Annu. Rev. Biophys. Biomol. Struct.* **1997**, *26*, 567−596.
(38) Plakhotnik, T.; Donley, E. A.; Wild, U. P. *Annu. Rev. Phys. Chem.* **1997**, *48*, 181−212.
(39) Xie, X. S.; Trautman, J. K. *Annu. Rev. Phys. Chem.* **1998**, *49*, 441−480.
(40) Moerner, W. E.; Dickson, R. M.; Norris, D. J. *Adv. At. Mol. Opt. Phys.* **1998**, *38*, 193−236.
(41) Meixner, A. J.; Kneppe, H. *Cell. Mol. Biol.* **1998**, *44*, 673−688.
(42) Weiss, S. *Science* **1999**, *283*, 1676−1683.

(43) Soper, S. A.; Nutter, H. L.; Keller, R. A. *Photochem. Photobiol.* **1993**, *57*, 972−977.
(44) Soper, S. A.; Lengendre, B. L.; Huang, J. *Chem. Phys. Lett.* **1995**, *237*, 339−345.
(45) Widengren, J.; Rigler, R. *Bioimaging* **1996**, *4*, 149−157.
(46) Eggeling, C.; Widengren, J.; Rigler, R.; Seidel, C. A. M. *Anal. Chem.* **1998**, *70*, 2651−2659.
(47) Eggeling, C.; Widengren, J.; Rigler, R.; Seidel, C. A. M. In *Applied Fluorescence in Chemistry, Biology and Medicine*; Rettig, W., Strehmel, B., Schrader, S., Seifert, H., Eds.; Springer-Verlag: Berlin, 1999; pp 195−240.
(48) Goodwin, P. M.; Ambrose, W. P.; Martin, J. C.; Keller, R. A. *Cytometry* **1995**, *21*, 133−144.
(49) Goodwin, P. M.; Affleck, R. L.; Ambrose, W. P.; Demas, J. N.; Jett, J. H.; Martin, J. C.; Reha-Krantz, L. J.; Semin, D. J.; Schecker, J. A.; Wu, M.; Keller, R. A. *Exp. Technol. Phys.* **1995**, *41*, 279−294.
(50) Kachel, V.; Fellner-Feldegg, H.; Menke, E. In *Flow Cytometry and Sorting*, 2nd ed.; Melamed, M. R., Lindmo, T., Mendelsohn, M. L., Eds.; J. Wiley & Sons: New York, 1990; pp 27−44.
(51) Zarrin, F.; Dovichi, N. J. *Anal. Chem.* **1985**, *57*, 2690−2692.
(52) Harris, T. D.; Lytle, F. E. In *Ultrasensitive Laser Spectroscopy*; Kliger, D. S., Ed.; Academic Press: New York, 1983; Chapter 7.
(53) Affleck, R. L.; Ambrose, W. P.; Demas, J. N.; Goodwin, P. M.; Schecker, J. A.; Wu, M.; Keller, R. A. *Anal. Chem.* **1996**, *68*, 2270−2276.
(54) Goodwin, P. M.; Wilkerson, C. W., Jr.; Ambrose, W. P.; Keller, R. A. *Proc. SPIE* **1993**, *1895*, 79−89.
(55) Peck, K.; Stryer, L.; Glazer, A. N.; Mathies, R. A. *Proc. Natl. Acad. Sci. U.S.A.* **1989**, *86*, 4087−4091.
(56) Wilkerson, C. W.; Goodwin, P. M.; Ambrose, W. P.; Martin, J. C.; Keller, R. A. *Appl. Phys. Lett.* **1993**, *62*, 2030−2032.
(57) Goodwin, P. M.; Affleck, R. L.; Ambrose, W. P.; Jett, J. H.; Johnson, M. E.; Martin, J. C.; Petty, J. T.; Schecker, J. A.; Wu, M.; Keller, R. A. In *Computer Assisted Analytical Spectroscopy*; Brown, S. D., Ed.; John Wiley and Sons: Chichester, England, 1996; pp 61−80.
(58) Tellinghuisen, J.; Goodwin, P. M.; Ambrose, W. P.; Martin, J. C.; Keller, R. A. *Anal. Chem.* **1994**, *66*, 64−72.
(59) Fries, J. R.; Brand, L.; Eggeling, C.; Köllner, M.; Seidel, C. A. M. *J. Phys. Chem. A* **1998**, *102*, 6601−6613.
(60) Machara, N. P.; Goodwin, P. M.; Enderlein, J.; Semin, D. J.; Keller, R. A. *Bioimaging* **1998**, *6*, 33−42.
(61) Davis, L. M.; Li, L.-Q. In *Laser Applications of Chemical Analysis*; Optical Society of America: Washington, DC, 1994. Davis, L. M.; Li, L.-Q. *OSA Technical Digest Series*; Optical Society of America: Washington, DC, 1994; Vol. 5, pp 206−209.
(62) Enderlein, J.; Robbins, D. L.; Ambrose, W. P.; Goodwin, P. M.; Keller, R. A. *J. Phys. Chem. B* **1997**, *101*, 3626−3632.
(63) Enderlein, J.; Robbins, D. L.; Ambrose, W. P.; Goodwin, P. M.; Keller, R. A. *Bioimaging* **1997**, *5*, 88−98.
(64) Lindmo, T.; Fundingsrud, K. *Cytometry* **1981**, *2*, 151−154.
(65) Soper, S. A.; Legendre, B. L., Jr. *Appl. Spectrosc.* **1998**, *52*, 1−6.
(66) Soper, S. A.; Davis, L. M.; Shera, E. B. *J. Opt. Soc. Am. B* **1992**, *9*, 1761−1769.
(67) Dörre, K.; Brakmann, S.; Brinkmeier, M.; Han, K.-T.; Riebeseel, K.; Schwille, P.; Stephan, J.; Wetzel, T.; Lapczyna, M.; Stuke, M.; Bader, R.; Hinz, M.; Seliger, H.; Holm, J.; Eigen, M.; Rigler, R. *Bioimaging* **1997**, *5*, 139−152.
(68) Tellinghuisen, J.; Wilkerson, C. W., Jr. *Anal. Chem.* **1993**, *65*, 1240−1246.
(69) Enderlein, J. *Exp. Technol. Phys.* **1991**, *39*, 479−486.
(70) Köllner, M.; Wolfrum, J. *J. Chem. Phys. Lett.* **1992**, *200*, 199−204.
(71) Köllner, M. *Appl. Opt.* **1993**, *32*, 806−820.
(72) Enderlein, J. *Proc. SPIE* **1994**, *2136*, 226−235.
(73) Enderlein, J. *Appl. Opt.* **1995**, *34*, 514−526.
(74) Enderlein, J.; Goodwin, P. M.; Van Orden, A.; Ambrose, W. P.; Erdmann, R.; Keller, R. A. *Chem. Phys. Lett.* **1997**, *270*, 464−470.
(75) Sauer, M.; Zander, C.; Müller, R.; Göbel, F.; Schultz, J.; Siebert, S.; Drexhage, K. H.; Wolfrum, J. *Proc. SPIE* **1997**, *2985*, 61−68.
(76) Müller, R.; Zander, C.; Sauer, M.; Deimel, M.; Ko, D. S.; Siebert, S.; Arden-Jacob, J.; Deltau, G.; Marx, N. J.; Drexhage, K. H.; Wolfrum, J. *Chem. Phys. Lett.* **1996**, *262*, 716−722.
(77) Sauer, M.; Zander, C.; Müller, R.; Ullrich, B.; Drexhage, K. H.; Kaul, S.; Wolfrum, J. *Appl. Phys. B* **1997**, *65*, 427−431.
(78) Sauer, M.; Arden-Jacob, J.; Drexhage, K. H.; Göbel, F.; Lieberwirth, U.; Mühlegger, K.; Müller, R.; Wolfrum, J.; Zander, C. *Bioimaging* **1998**, *6*, 14−24.
(79) Van Orden, A.; Machara, N. P.; Goodwin, P. M.; Keller, R. A. *Anal. Chem.* **1998**, *70*, 1444−1451.
(80) Schaffer, J.; Volkmer, A.; Eggeling, C.; Subramaniam, V.; Striker, G.; Seidel, C. A. M. *J. Phys. Chem. A* **1999**, *103*, 332−336.
(81) Jett, J. H.; Keller, R. A.; Martin, J. C.; Marrone, B. L.; Moyzis, R. K.; Ratliff, R. L.; Seitzinger, N. K.; Shera, E. B.; Stewart, C. C. *J. Biomol. Struct. Dynam.* **1989**, *7*, 301−309.
(82) Jett, J. H.; Keller, R. A.; Martin, J. C.; Moyzis, R. K.; Ratliff, R. L.; Shera, E. B.; Stewart, C. C. U.S. Patent 4,962,137, 1990.
(83) Ambrose, W. P.; Goodwin, P. M.; Jett, J. H.; Johnson, M. E.; Martin, J. C.; Marrone, B. L.; Schecker, J. A.; Wilkerson, C. W.; Keller, R. A. *Ber. Bunsen-Ges. Phys. Chem.* **1993**, *97*, 1535−1542.
(84) Eigen, M.; Rigler, R. *Proc. Natl. Acad. Sci. U.S.A.* **1994**, *91*, 5740−5747.
(85) Jett, J. H.; Hammond, M. L.; Keller, R. A.; Martin, J. C.; Posner, R. G.; Marrone, B. L.; Simpson, D. J. U.S. Patent 5,405,747, 1995.
(86) Schecker, J. A.; Goodwin, P. M.; Affleck, R. L.; Wu, M.; Martin, J. C.; Jett, J. H.; Keller, R. A. *Proc. SPIE* **1995**, *2386*, 4−12.
(87) Goodwin, P. M.; Cai, H.; Jett, J. H.; Ishaug-Riley, S. L.; Machara, N. P.; Semin, D. J.; Van Orden, A.; Keller, R. A. *Nucleosides Nucleotides* **1997**, *16*, 543−550.
(88) Dapprich, J.; Nicklaus, N. *Bioimaging* **1998**, *6*, 25−32.
(89) Werner, J. H.; Cai, H.; Goodwin, P. M.; Keller, R. A. *Proc. SPIE* **1999**, *3602*, 355−366.
(90) Castro, A.; Fairfield, F. R.; Shera, E. B. *Anal. Chem.* **1993**, *65*, 849−852.
(91) Goodwin, P. M.; Johnson, M. E.; Martin, J. C.; Ambrose, W. P.; Jett, J. H.; Keller, R. A. *Nucleic Acids Res.* **1993**, *21*, 803−806.
(92) Johnson, M. E.; Goodwin, P. M.; Ambrose, W. P.; Martin, J. C.; Marrone, B. L.; Jett, J. H.; Keller, R. A. *Proc. SPIE* **1993**, *1895*, 69−78.
(93) Petty, J. T.; Johnson, M. E.; Goodwin, P. M.; Martin, J. C.; Jett, J. H.; Keller, R. A. *Anal. Chem.* **1995**, *67*, 1755−1761.
(94) Huang, Z.; Petty, J. T.; O'Quinn, B.; Longmire, J. L.; Brown, N. C.; Jett, J. H.; Keller, R. A. *Nucleic Acids Res.* **1996**, *24*, 4202−4209.
(95) Huang, Z.; Jett, J. H.; Keller, R. A. *Cytometry* **1999**, *35*, 169−175.
(96) Habbersett, R. C.; Jett, J. H.; Keller, R. A. In *Emerging Tools for Cell Analysis: Advances in Optical Measurement*; J. Wiley and Sons: New York, 1999, in press.
(97) Kim, Y.; Jett, J. H.; Larson, E. J.; Penttila, J. R.; Marrone, B. L.; Keller, R. A. *Cytometry* **1999**, *36*, 1−9.
(98) Ambrose, W. P.; Cai, H.; Goodwin, P. M.; Jett, J. H.; Habbersett, R. C.; Larson, E. J.; Grace, W. K.; Werner, J. H.; Keller, R. A. In *Topics in Fluorescence: DNA Technology*; Lakowicz, J. R., Ed.; Plenum: New York, 1999; Vol. 7, in press.
(99) Glazer, A. N.; Rye, H. S. *Nature* **1992**, *359*, 859−861.
(100) Agronskaia, A.; Schins, J. M.; de Grooth, B. G.; Greve, J. *Appl. Opt.* **1999**, *38*, 714−719.
(101) Ioannou, P. A.; Amemiva, C. T.; Garnes, J.; Kroisel, P. I.; Shizuya, H.; Chen, C.; Batzer, M. A.; DeJong, P. J. *Nat. Genet.* **1994**, *6*, 84−89.
(102) Castro, A.; Williams, J. G. K. *Anal. Chem.* **1997**, *69*, 3915−3920.
(103) Haab, B. B.; Mathies, R. A. *Anal. Chem.* **1995**, *67*, 3253−3260.
(104) Haab, B. B.; Mathies, R. A. *Appl. Spectrosc.* **1997**, *51*, 1579−1584.
(105) Fister, J. C.; Jacobson, S. C.; Davis, L. M.; Ramsey, J. M. *Anal. Chem.* **1998**, *70*, 431−437.
(106) Whitten, W. B.; Ramsey, J. M.; Arnold, S.; Bronk, B. V. *Anal. Chem.* **1991**, *63*, 1027−1031.
(107) Ng, K. C.; Whitten, W. B.; Arnold, S.; Ramsey, J. M. *Anal. Chem.* **1992**, *64*, 2914−2919.
(108) Mahoney, P. P.; Hieftje, G. M. *Appl. Spectrosc.* **1994**, *48*, 956−958.
(109) Lermer, N.; Barnes, M. D.; Kung, C.-Y.; Whitten, W. B.; Ramsey, J. M. *Anal. Chem.* **1997**, *69*, 2115−2121.
(110) Barnes, M. D.; Lermer, N.; Kung, C.-Y.; Whitten, W. B.; Ramsey, J. M.; Hill, S. C. *Opt. Lett.* **1997**, *22*, 1265−1267.
(111) Kung, C.-Y.; Barnes, M. D.; Lermer, N.; Whitten, W. B.; Ramsey, J. M. *Anal. Chem.* **1998**, *70*, 658−661.
(112) Hill, S. C.; Saleheen, H. I.; Barnes, M. D.; Whitten, W. B.; Ramsey, J. M. *Appl. Opt.* **1996**, *35*, 6278−6288.
(113) Hill, S. C.; Barnes, M. D.; Whitten, W. B.; Ramsey, J. M. *Appl. Opt.* **1997**, *36*, 4425−4437.
(114) Lermer, N.; Barnes, M. D.; Kung, C.-Y.; Whitten, W. B.; Ramsey, J. M. *Opt. Lett.* **1998**, *23*, 951−953.
(115) Rigler, R.; Mets, Ü. *Proc. SPIE* **1992**, ***1921***, 239−248.
(116) Mets, Ü.; Rigler, R. *J. Fluoresc.* **1994**, *4*, 259−264.
(117) Nie, S.; Chiu, D. T.; Zare, R. N. *Anal. Chem.* **1995**, *67*, 2849−2857.
(118) Chiu, D. T.; Zare, R. N. *J. Am. Chem. Soc.* **1996**, *118*, 6512−6513.
(119) Edman, L.; Mets, Ü.; Rigler, R. *Exp. Technol. Phys.* **1995**, *41*, 157−163.
(120) Edman, L.; Mets, Ü.; Rigler, R. *Proc. Natl. Acad. Sci. U.S.A.* **1996**, *93*, 6710−6715.
(121) Eggeling, C.; Fries, J. R.; Brand, L.; Günther, R.; Siedel, C. A. M. *Proc. Natl. Acad. Sci. U.S.A.* **1998**, *95*, 1556−1561.
(122) Edman, L.; Wennmalm, S.; Tamsen, F.; Rigler, R. *Chem. Phys. Lett.* **1998**, *292*, 15−21.
(123) Maiti, S.; Haupts, U.; Webb, W. W. *Proc. Natl. Acad. Sci. U.S.A.* **1997**, *94*, 11753−11757.

(124) Thompson, N. L. In *Topics in Fluorescence Spectroscopy*; Lakowicz, J. R., Ed.; Plenum Press: New York, 1991; Vol. 1, pp 337−378.
(125) Magde, D.; Elson, E. L.; Webb, W. W. *Phys. Rev. Lett.* **1972**, *29*, 705−708.
(126) Elson, E. L.; Magde, D. *Biopolymers* **1974**, *13*, 1−28.
(127) Magde, D.; Elson, E. L.; Webb, W. W. *Biopolymers* **1974**, *13*, 29−61.
(128) Ehrenberg, M.; Rigler, R. *Chem. Phys.* **1974**, *4*, 390−401.
(129) Aragón, S. R.; Pecora, R. *Biopolymers* **1975**, *14*, 119−137.
(130) Aragón, S. R.; Pecora, R. *J. Chem. Phys.* **1976**, *64*, 1791−1803.
(131) Briggs, J.; Elings, V. B.; Nicoli, D. F. *Science* **1981**, *212*, 1266−1267.
(132) Rauer, B.; Neumann, E.; Widengren, J.; Rigler, R. *Biophys. Chem.* **1996**, *58*, 3−12.
(133) Van Orden, A.; Keller, R. A. *Anal. Chem.* **1998**, *70*, 4463−4471.
(134) Schwille, P.; Bieschke, J.; Oehlenschläger, F. *Biophys. Chem.* **1997**, *66*, 211−228.
(135) Rigler, R.; Mets, Ü.; Widengren, J.; Kask, P. *Eur. Biophys. J.* **1993**, *22*, 169−175.
(136) Rigler, R. *J. Biotechnol.* **1995**, *41*, 177−186.
(137) Kinjo, M.; Rigler, R. *Nucleic Acids Res.* **1995**, *23*, 1795−1799.
(138) Schwille, P.; Oehlenschläger, F.; Walter, N. G. *Biochemistry* **1996**, *35*, 10182−10193.
(139) Földes-Papp, Z.; Thyberg, P.; Björling, S.; Holmgren, A.; Rigler, R. *Nucleotides Nucleosides* **1997**, *16*, 781−787.
(140) Nishimura, G.; Rigler, R.; Kinjo, M. *Bioimaging* **1997**, *5*, 129−133.
(141) Kinjo, M.; Nishimura, G.; Koyama, T.; Mets, Ü.; Rigler, R. *Anal. Biochem.* **1998**, *260*, 166−172.
(142) Björling, S.; Kinjo, M.; Földes-Papp, Z.; Hagman, E.; Thyberg, P.; Rigler, R. *Biochemistry* **1998**, *37*, 12971−12978.
(143) Kinjo, M.; Nishimura, G. *Bioimaging* **1997**, *5*, 134−138.
(144) Kinjo, M. *Anal. Chim. Acta* **1998**, *365*, 43−48.
(145) Huapts, U.; Maiti, S.; Schwille, P.; Webb, W. W. *Proc. Natl. Acad. Sci. U.S.A.* **1998**, *95*, 13573−13578.
(146) La Clair, J. J. *J. Am. Chem. Soc.* **1997**, *119*, 7676−7684.
(147) Börsch, M.; Turina, P.; Eggeling, C.; Fries, J. R.; Seidel, C. A. M.; Labahn, A.; Gräber, P. *FEBS Lett.* **1998**, *437*, 251−254.
(148) Dorn, I. T.; Neumaier, K. R.; Tampé, R. J. *Am. Chem. Soc.* **1998**, *120*, 2753−2763.
(149) Widengren, J.; Rigler, R.; Mets, Ü. *J. Fluoresc.* **1994**, *4*, 255−258.
(150) Widengren, J.; Mets, Ü.; Rigler, R. *J. Phys. Chem.* **1995**, *99*, 13368−13379.
(151) Widengren, J.; Dapprich, J.; Rigler, R. *Chem. Phys.* **1997**, *216*, 417−426.
(152) Schwille, P.; Meyer-Almes, F. J.; Rigler, R. *Biophys. J.* **1997**, *72*, 1878−1886.
(153) Rigler, R.; Földes-Papp, Z.; Meyer-Almes, F. J.; Sammet, C.; Völcker, M.; Schnetz, A. *J. Biotechnol.* **1998**, *63*, 97−102.
(154) Kettling, U.; Koltermann, A.; Schwille, P.; Eigen, M. *Proc. Natl. Acad. Sci. U.S.A.* **1998**, *95*, 1416−1420.
(155) Koltermann, A.; Kettling, U.; Bieschke, J.; Winkler, T.; Eigen, M. *Proc. Natl. Acad. Sci. U.S.A.* **1998**, *95*, 1421−1426.
(156) Guenard, R. D.; King, L. A.; Smith, B. W.; Winefordner, J. D. *Anal. Chem.* **1997**, *69*, 2426−2433.
(157) Mathis, H. P.; Kalusche, G.; Wagner, B.; McCaskill, J. S. *Bioimaging* **1997**, *5*, 116−128.
(158) Lyon, W. A.; Nie, S. *Anal. Chem.* **1997**, *69*, 3400−3405.
(159) Zander, C.; Drexhage, K. H. *Proc. SPIE* **1997**, *2980*, 545−550.
(160) Zander, C.; Drexhage, K. H.; Han, K.-T.; Wolfrum, J.; Sauer, M. *Chem. Phys. Lett.* **1998**, *286*, 457−465.
(161) Plakhotnik, T.; Walser, D.; Pirotta, M.; Renn, A.; Wild, U. P. *Science* **1996**, *271*, 1703−1705.
(162) Brand, L.; Eggeling, C.; Zander, C.; Drexhage, K. H.; Seidel, C. A. M. *J. Phys. Chem. A* **1997**, *101*, 4313−4321.
(163) Sánchez, E. J.; Novotny, L.; Holtom, G. R.; Xie, X. S. *J. Phys. Chem. A* **1997**, *101*, 7019−7023.
(164) Bopp, M. A.; Jia, Y.; Haran, G.; Morlino, E. A.; Hochstrasser, R. M. *Appl. Phys. Lett.* **1998**, *73*, 7−9.
(165) Lewis, M. K.; Wolanin, P.; Gafni, A.; Steel, D. G. *Opt. Lett.* **1998**, *23*, 1111−1113.
(166) Song, J. M.; Inoue, T.; Kawazumi, H.; Ogawa, T. *Anal. Sci.* **1998**, *14*, 913−916.
(167) Denk, W.; Strickler, J. H.; Webb, W. W. *Science* **1990**, *248*, 73−76.
(168) So, P. T. C.; Konig, K.; Berland, K.; Dong, C. Y.; French, T.; Buhler, C.; Ragan, T.; Gratton, E. *Cell. Mol. Biol.* **1998**, *44*, 771−793.
(169) Xu, C.; Webb, W. W. *J. Opt. Soc. Am. B* **1995**, *13*, 481−491.
(170) Overway, K. S.; Duhachek, S. D.; Loeffel-Mann, K.; Zugel, S. A.; Lytle, F. E. *Appl. Spectrosc.* **1996**, *50*, 1335−1337.
(171) Shear, J. B.; Brown, E. B.; Webb, W. W. *Anal. Chem.* **1996**, *68*, 1778−1783.
(172) Zander, C.; Brand, L.; Eggeling, C.; Drexhage, K. H.; Seidel, C. A. M. *Proc. SPIE* **1997**, *2980*, 552−558.
(173) Brand, L.; Eggeling, C.; Seidel, C. A. M. *Nucleosides Nucleotides* **1997**, *16*, 551−556.
(174) Xu, C.; Shear, J. B.; Webb, W. W. *Anal. Chem.* **1997**, *69*, 1285−1287.
(175) Berland, K. M.; Cho, P. T. C.; Gratton, E. *Biophys. J.* **1995**, *68*, 694−701.
(176) Berland, K. M.; Cho, P. T. C.; Chen, Y.; Mantulin, W. W.; Gratton, E. *Biophys. J.* **1996**, *71*, 410−420.
(177) Plakhotnik, T.; Walser, D.; Renn, A.; Wild, U. P. *Phys. Rev. Lett.* **1996**, *77*, 5365−5368.
(178) Plakhotnik, T.; Walser, D. *Phys. Rev. Lett.* **1998**, *80*, 4064−4067.
(179) Bhawalker, J. D.; He, G. S.; Park, C. K.; Zhao, C. F.; Ruland, G.; Prasad, P. N. *Opt. Commun.* **1996**, *124*, 33−37.
(180) Albota, M.; Beljonne, D.; Bredas, J. L.; Ehrlich, J. E.; Fu, J. Y.; Heikal, A. A.; Hess, S. E.; Kogej, T.; Levin, M. D.; Marder, S. R.; McCord-Maughon, D.; Perry, J.; Röckel, H.; Rumi, M.; Subramaniam, G.; Webb, W. W.; Wu, X. L.; Xu, C. *Science* **1998**, *281*, 1653−1656.
(181) Güttler, F.; Irngartinger, T.; Plakhotnik, T.; Renn, A.; Wild, U. P. *Chem. Phys. Lett.* **1994**, *217*, 393.
(182) Tchénio, P.; Myers, A. B.; Moerner, W. E. *J. Phys. Chem.* **1993**, *97*, 2491−2493.
(183) Ishikawa, M.; Watanabe, M.; Hayakawa, T.; Koishi, M. *Anal. Chem.* **1995**, *67*, 511−518.
(184) Fleury, L.; Tamarat, P.; Lounis, B.; Bernard, J.; Orrit, M. *Chem. Phys. Lett.* **1995**, *236*, 87−95.
(185) Macklin, J. J.; Trautman, J. K.; Harris, T. D.; Brus, L. E. *Science* **1996**, *272*, 255−258.
(186) Lu, H. P.; Xie, X. S. *Nature* **1997**, *385*, 143.
(187) Nie, S.; Emory, S. R. *Science* **1997**, *275*, 1102−1106.
(188) Kneipp, K.; Wang, Y.; Kneipp, H.; Perelman, L. T.; Itzkan, I.; Dasari, R. R.; Feld, M. S. *Phys. Rev. Lett.* **1997**, *78*, 1667−1670.
(189) Mais, S.; Tittel, J.; Basché, T.; Bräuchle, C.; Göhde, W.; Fuchs, H.; Müller, G.; Müllen, K. *J. Phys. Chem. A* **1997**, *101*, 8435−8440.
(190) Weston, K. D.; Carson, P. J.; Metiu, H.; Buratto, S. K. *J. Chem. Phys.* **1998**, *109*, 7474−7485.
(191) Ye, J. Y.; Ishikawa, M.; Yogi, O.; Okada, T.; Maruyama, Y. *Chem. Phys. Lett.* **1998**, *288*, 885−890.
(192) Vale, R. D.; Funatsu, T.; Pierce, D. W.; Romberg, L.; Harada, Y.; Yanagida, T. *Nature* **1996**, *380*, 451−453.
(193) Schmidt, T.; Schütz, G. J.; Gruber, H. J.; Schindler, H. *Anal. Chem.* **1996**, *68*, 4397−4401.
(194) Schmidt, T.; Schütz, G. J.; Baumgartner, W.; Gruber, H. J.; Schindler, H. *Proc. Natl. Acad. Sci. U.S.A.* **1996**, *93*, 2926−2929.
(195) Ishijima, A.; Kojima, H.; Higuchi, H.; Harada, Y.; Funatsu, T.; Yanagida, T. *Biophys. J.* **1996**, *70*, 383−400.
(196) Miyata, H.; Yasuda, R.; Kinosita, K. *Biochim. Biophys. Acta* **1996**, *1290*, 83−88.
(197) Dickson, R. M.; Cubitt, A. B.; Tsien, R. Y.; Moerner, W. E. *Nature* **1997**, *388*, 355−358.
(198) Funatsu, T.; Harada, Y.; Higuchi, H.; Tokunaga, M.; Saito, K.; Ishii, Y.; Vale, R. D.; Yanagida, T. *Biophys. Chem.* **1997**, *68*, 63−72.
(199) Noji, H.; Yasuda, R.; Yoshida, M.; Kinosita, K. *Nature* **1997**, *386*, 299−302.
(200) Iwane, A. H.; Funatsu, T.; Harada, Y.; Tokunaga, M.; Ohara, O.; Morimoto, S.; Yanagida, T. *FEBS Lett.* **1997**, *407*, 235−238.
(201) Schütz, G. J.; Schindler, H.; Schmidt, T. *Biophys. J.* **1997**, *73*, 1073−1080.
(202) Schütz, G. J.; Gruber, H. J.; Schindler, H.; Schmidt, T. *J. Lumin.* **1997**, *72*, 18−21.
(203) Schütz, G. J.; Schindler, H.; Schmidt, T. *Opt. Lett.* **1997**, *22*, 651−653.
(204) Tan, W. H.; Yeung, E. S. *Anal. Chem.* **1997**, *69*, 4242−4248.
(205) Tokunaga, M.; Kitamura, K.; Saito, K.; Iwane, A. H.; Yanagida, T. *Biochem. Biophys. Res. Commun.* **1997**, *235*, 47−53.
(206) Saito, K.; Tokunaga, M.; Iwane, A. H.; Yanagida, T. *J. Microsc.* **1997**, *188*, 255−263.
(207) Yasuda, R.; Noji, H.; Kinosita, K.; Motojima, F.; Yoshida, M. *J. Bioenerg. Biomembr.* **1997**, *29*, 207−209.
(208) Sase, I.; Miyata, H.; Ishiwata, S.; Kinosita, K. *Proc. Natl. Acad. Sci. U.S.A.* **1997**, *94*, 5646−5650.
(209) Semin, D. J.; Ambrose, W. P.; Goodwin, P. M.; Wendt, J. R.; Keller, R. A. *Proc. SPIE* **1997**, *3009*, 109−118.
(210) Harada, Y.; Funatsu, T.; Tokunaga, M.; Saito, K.; Higuchi, H.; Ishii, Y.; Yanagida, T. *Methods Cell Biol.* **1998**, *55*, 117−128.
(211) Ishijima, A.; Kojima, H.; Funatsu, T.; Tokunaga, M.; Higuchi, H.; Tanaka, H.; Yanagida, T. *Cell* **1998**, *92*, 161−171.
(212) Ishikawa, M.; Yogi, O.; Ye, J. Y.; Yasuda, T.; Maruyama, Y. *Anal. Chem.* **1998**, *70*, 5198−5208.
(213) Schütz, G. J.; Trabesinger, W.; Schmidt, T. *Biophys. J.* **1998**, *74*, 2223−2226.
(214) Yasuda, R.; Nohi, H.; Kinosita, K.; Yoshida, M. *Cell* **1998**, *93*, 1117−1124.
(215) Yokota, H.; Saito, K.; Yanagida, T. *Phys. Rev. Lett.* **1998**, *80*, 4606−4609.
(216) Xu, X.-H. N.; Yeung, E. S. *Science* **1998**, *281*, 1650−1653.

(217) Dickson, R. M.; Norris, D. J.; Moerner, W. E. *Phys. Rev. Lett.* **1998**, *81*, 5322−5325.
(218) Trabesinger, W.; Schutz, G. J.; Gruber, H. J.; Schindler, H.; Schmidt, T. *Anal. Chem.* **1999**, *71*, 279−283.
(219) Harada, Y.; Funatsu, T.; Murakami, K.; Nonoyama, Y.; Ishihama, A.; Yanagida, T. *Biophys. J.* **1999**, *76*, 709−715.
(220) Ambrose, W. P.; Goodwin, P. M.; Nolan, J. P. *Cytometry* **1999**, *36*, 224−231.
(221) Ha, T.; Enderle, T.; Chemla, D. S.; Selvin, P. R.; Weiss, S. *Phys. Rev. Lett.* **1996**, *77*, 3979.
(222) Ruiter, A. G. T.; Veerman, J. A.; Garcia-Parajo, M. F.; vanHulst, N. F. *J. Phys. Chem. A* **1997**, *101*, 7318−7323.
(223) Ambrose, W. P.; Goodwin, P. M.; Enderlein, J.; Semin, D. J.; Keller, R. A. *Proc. SPIE* **1998**, *3270*, 190−199.
(224) Ha, T.; Enderle, T.; Chemla, D. S.; Weiss, S. *IEEE J. Sel. Top. Quantum Electron.* **1996**, *2*, 1115−1128.
(225) Ambrose, W. P.; Goodwin, P. M.; Martin, J. C.; Keller, R. A. *Science* **1994**, *265*, 364−367.
(226) Ambrose, W. P.; Affleck, R. L.; Goodwin, P. M.; Keller, R. A.; Martin, J. C.; Petty, J. T.; Schecker, J. A.; Wu, M. *Exp. Technol. Phys.* **1995**, *41*, 237−248.
(227) Meixner, A. J.; Zeisel, D.; Bopp, M. A.; Tarrach, G. *Opt. Eng.* **1996**, *34*, 2324−2332.
(228) Ambrose, W. P.; Goodwin, P. M.; Enderlein, J.; Semin, D. J.; Martin, J. C.; Keller, R. A. *Chem. Phys. Lett.* **1997**, *269*, 365−370.
(229) Drexhage, K. H. In *Progress in Optics XII*; Wolf, E., Ed.; North-Holland: Amsterdam, 1974; pp 163−232.
(230) Axelrod, D. *Methods Cell Biol.* **1989**, *30*, 245−270.
(231) Lu, H. P.; Xun, L. Y.; Xie, X. S. *Science* **1998**, *282*, 1877−1882.
(232) Block, S. M. *Cell* **1998**, *93*, 5−8.
(233) Tsien. In *Handbook of Biological Confocal Microscopy*, 2nd ed.; Pawley, J. B., Ed.; Plenum Press: New York, 1995; Chapter 16.
(234) Marinesco, N. S. *J. Chim. Phys.* **1927**, *24*, 593−620.

CR980132Z